Inorganic Chemistry
Article

Inorg. Chem. **2011**, *50*, 621–635 **621**
DOI: 10.1021/ic1018136

Synthesis, Structure, and DNA Cleavage Properties of Copper(II) Complexes of 1,4,7-Triazacyclononane Ligands Featuring Pairs of Guanidine Pendants

Linda Tjioe,[†] Tanmaya Joshi,[†] Joël Brugger,[‡,§] Bim Graham,*[,⊥] and Leone Spiccia*[,†]

[†]*School of Chemistry, Monash University, Vic 3800, Australia,* [‡]*School of Earth & Environmental Science, University of Adelaide, Adelaide, SA 5005 Australia,* [§]*South Australian Museum, Adelaide, SA 5000, Australia, and* [⊥]*Medicinal Chemistry and Drug Action, Monash Institute of Pharmaceutical Sciences, Monash University, Parkville, Vic 3052, Australia*

Received September 3, 2010

Two new ligands, $\mathbf{L^1}$ and $\mathbf{L^2}$, have been prepared via N-functionalization of 1,4,7-triazacyclononane (tacn) with pairs of ethyl- or propyl-guanidine pendants, respectively. The X-ray crystal structure of $[Cu\mathbf{L^1}](ClO_4)_2$ (**C1**) isolated from basic solution (pH 9) indicates that a secondary amine nitrogen from each guanidine pendants coordinates to the copper(II) center in addition to the nitrogen atoms in the tacn macrocycle, resulting in a five-coordinate complex with intermediate square-pyramidal/trigonal bipyramidal geometry. The guanidines adopt an unusual coordination mode in that their amine nitrogen nearest to the tacn macrocycle binds to the copper(II) center, forming very stable five-membered chelate rings. A spectrophotometric pH titration established the pK_{app} for the deprotonation and coordination of each guanidine group to be 3.98 and 5.72, and revealed that $[Cu\mathbf{L^1}]^{2+}$ is the only detectable species present in solution above pH ~8. The solution speciation of the $Cu\mathbf{L^2}$ complex (**C2**) is more complex, with at least 5 deprotonation steps over the pH range 4−12.5, and mononuclear and binuclear complexes coexisting. Analysis of the spectrophotometric data provided apparent deprotonation constants, and suggests that solutions at pH ~7.5 contain the maximum proportion of polynuclear complexes. Complex **C1** exhibits virtually no cleavage activity toward the model phosphate diesters, *bis*(*p*-nitrophenyl)phosphate (BNPP) and 2-hydroxypropyl-*p*-nitrophenyl phosphate (HPNPP), while **C2** exhibits moderate activity. For **C2**, the respective k_{obs} values measured at pH 7.0 ($7.24\ (\pm 0.08) \times 10^{-5}\ s^{-1}$ (BNPP at 50 °C) and $3.2\ (\pm 0.3) \times 10^{-5}\ s^{-1}$ (HPNPP at 25 °C)) are 40- and 10-times faster than $[Cu(tacn)(OH_2)_2]^{2+}$ complex. Both complexes cleave supercoiled pBR 322 plasmid DNA, indicating that the guanidine pendants of $[Cu\mathbf{L^1}]^{2+}$ may have been displaced from the copper coordination sphere to allow for DNA binding and subsequent cleavage. The rate of DNA cleavage by **C2** is twice that measured for $[Cu(tacn)(OH_2)_2]^{2+}$, suggesting some degree of cooperativity between the copper center and guanidinium pendants in the hydrolysis of the phosphate ester linkages of DNA. A predominantly hydrolytic cleavage mechanism was confirmed through experiments performed either in the presence of various radical scavengers or under anaerobic conditions.

Introduction

The Human Genome Project has found that the human genome consists of 20 000−25 000 protein-coding genes, which are transcribed into the messenger ribonucleic acids (mRNA) responsible for protein synthesis.[1] Since even a single mutation in any of these genes, or loss of an mRNA or protein, can have serious implications, nature utilizes kinetically inert linkages to connect the key components, *viz*., phosphodiester and peptide bonds in RNA/DNA and proteins, respectively. This inertness is highlighted by the half-life for the uncatalyzed cleavage of phosphate ester bonds in DNA (10^5 years at pH 7, 25 °C).[2] However, processes that either attach or detach phosphate groups from biological molecules underpin many fundamental biological processes.[3−6] Since the uncatalyzed rates of cleavage of such groups from biological molecules are too slow to sustain life, enzymes (protein-based, as well as ribozymes) are used to promote phosphoryl transfer reactions in the biological arena.[7,8]

*To whom correspondence should be addressed. E-mail: Bim.Graham@pharm.monash.edu.au (B.G.); Leone.Spiccia@monash.edu (L.S.). Fax: +61 3 9903 9582 (B.G.); +61 3 9905 4597 (L.S.).

(1) International Human Genome Sequencing Consortium *Nature* **2001**, *409*, 860–921.
(2) Radzicka, A.; Wolfenden, R. *Science* **1995**, *267*, 90–93.
(3) Trawick, B. N.; Daniher, A. T.; Bashkin, J. K. *Chem. Rev.* **1998**, *98*, 939–960.
(4) Gani, D.; Wilkie, J. *Structure and Bonding*; Springer: Berlin, Germany, 1997.
(5) Strater, N.; Lipscomb, W. N.; Klabunde, T.; Krebs, B. *Angew. Chem., Int. Ed. Engl.* **1996**, *35*, 2024–2055.
(6) Hegg, E. L.; Burstyn, J. N. *Coord. Chem. Rev.* **1998**, *173*, 133–165.
(7) Cotton, F. A.; Hazen, E. E. J.; Legg, M. *Proc. Natl. Acad. Sci. U.S.A.* **1979**, *76*, 2551–2555.
(8) Weber, D. J.; Meeker, A. K.; Mildvan, A. S. *Biochemistry* **1991**, *30*, 6103–6114.

Published on Web 12/09/2010

A key feature of many (ribo)nucleases and phosphatases is the presence of one or more metal ions within the active sites of these enzymes that is crucial for activity. These ions facilitate phosphate cleavage/phosphoryl group transfer in a variety of ways: (i) Lewis acid activation of the substrate through coordination to the metal ion(s); (ii) provision of metal-bound hydroxide or alkoxide groups to serve as nucleophiles or bases; (iii) stabilization of transition states; and (iv) assisting the departure of leaving groups. Functional groups of amino acid side chains present within the enzyme active sites serve to synergistically reinforce the catalytic action of these metal ions. A good example is provided by the well-studied enzyme alkaline phosphatase (AP), which uses two zinc centers, in conjunction with key serine and arginine residues, to help promote the rapid cleavage of phosphate monoesters.[9] The positively charged guanidinium group present in arginine is postulated to assist with substrate activation and transition state stabilization, while the serine residue provides the attacking nucleophile, leading to the formation of a phosphoserinyl intermediate during AP's catalytic cycle.

Inspired by the occurrence of metal-containing (ribo)-nucleases and phosphatases, many research groups have sought to develop low-molecular weight metal complexes that are able to cleave biologically important phosphate esters.[6,10−15] This research has been stimulated by the realization that small, hydrolytically active metal complexes (and their conjugates with various targeting agents) may potentially find utility as artificial restriction enzymes in molecular biology research, and as nucleic acid-targeting therapeutics.[16−36]

Many of the first generation enzyme mimics were simple mononuclear chelate complexes featuring bidentate or tridentate ligands, such as bipyridine (bipy), 1,4,7-triazacyclononane (tacn), and *bis*(2-pyridylmethyl)amine (BPA or DPA).[36−47] More recently, increasing attention has been paid to the design and synthesis of more sophisticated supporting ligand structures featuring auxiliary amino, ammonium and guanidinium groups.[34,39,40,48−59] These yield complexes that mimic the cooperativity between metal ions and key amino acid residues found within the active sites of the metalloenzymes, and which generally cleave model phosphate esters or nucleic acids significantly more rapidly than their non-functionalized counterparts. Krämer and co-workers,[39,40] for example, showed that the copper(II) complex of a bipy-based ligand with inbuilt ammonium groups (Figure 1A) cleaves a model phosphate diester 2900-times faster than the complex of the corresponding ligand without hydrogen bond donors. More recently, Chin and co-workers[41] have reported a copper(II) complex with two amino groups (Figure 1B) in close proximity to the metal center which accelerates the rate of hydrolysis of 2′-3′-cyclic adenosine monophosphate (cAMP) by a factor of 2×10^7. Our group has studied the DNA cleavage activity of a series of copper(II) complexes of

(9) Wilcox, D. E. *Chem. Rev.* **1996**, *96*, 2435–2458.
(10) Yun, J. W.; Tanase, T.; Lippard, S. J. *Inorg. Chem.* **1996**, *35*, 7590–7600.
(11) Gomez-Tagle, P.; Yatsimirsky, A. K. *J. Chem. Soc., Dalton Trans.* **2001**, 2663–2670.
(12) Hay, R. W.; Govan, N. *Polyhedron* **1998**, *17*, 463–468.
(13) Hegg, E. L.; Burstyn, J. N. *J. Am. Chem. Soc.* **1995**, *117*, 7015–7016.
(14) Hegg, E. L.; Burstyn, J. N. *Inorg. Chem.* **1996**, *35*, 7474–7481.
(15) Hegg, E. L.; Deal, K. A.; Kiessling, L. L.; Burstyn, J. N. *Inorg. Chem.* **1997**, *36*, 1715–1718.
(16) Erkkila, K. E.; Odom, D. T.; Barton, J. K. *Chem. Rev.* **1999**, *99*, 2777–2796.
(17) Rajski, S. R.; Williams, R. M. *Chem. Rev.* **1998**, *98*, 2723–2796.
(18) Burger, R. M. *Chem. Rev.* **1998**, *98*, 1153–1170.
(19) Sherman, S. E.; Lippard, S. J. *Chem. Rev.* **1987**, *87*, 1153–1181.
(20) Cowan, J. A. *Curr. Opin. Chem. Biol.* **2001**, *5*, 634–642.
(21) Morrow, J. R.; Iranzo, O. *Curr. Opin. Chem. Biol.* **2004**, *8*, 192–200.
(22) Baker, B. F.; Lot, S. S.; Kringle, J.; Cheng-Flournoy, S.; Villiet, P.; Sasmor, H. M.; Siskowski, A. M.; Chappell, L. L.; Morrow, J. R. *Nucl. Acids. Res.* **1999**, *27*, 1547–1551.
(23) Perreault, D. M.; Ansyln, E. V. *Angew. Chem., Int. Ed.* **1997**, *36*, 432–450.
(24) Cheng, C. C.; Rokita, S. E.; Burrows, C. J. *Angew. Chem., Int. Ed.* **1993**, *32*, 277–278.
(25) Friedel, M. G.; Pieck, J. C.; Klages, J.; Dauth, C.; Kessler, H.; Carell, T. *Chem.—Eur. J.* **2006**, *12*, 6081–6094.
(26) Mancin, F.; Tecilla, P. *New. J. Chem.* **2007**, *31*, 800–817.
(27) Noll, D. M.; Mason, T. M.; Miller, P. S. *Chem. Rev.* **2006**, *106*, 277–301.
(28) Hettich, R.; Schneider, H.-J. *J. Am. Chem. Soc.* **1997**, *119*, 5638–5647.
(29) Ren, R.; Yang, P.; Zheng, W.; Hua, Z. *Inorg. Chem.* **2000**, *39*, 5454–5463.
(30) Komiyama, M.; Kina, S.; Matsumura, K.; Sumaoka, J.; Tobey, S.; Lynch, V. M.; Ansyln, E. V. *J. Am. Chem. Soc.* **2002**, *124*, 13731–13736.
(31) Yang, M.-Y.; Richard, J. P.; Morrow, J. R. *Chem. Commun.* **2003**, 2832–2833.
(32) Worm, K.; Chu, F.; Matsumoto, K.; Best, M. D.; Lynch, V. M.; Ansyln, E. V. *Chem.—Eur. J.* **2003**, *9*, 741–747.
(33) Jin, Y.; Cowan, J. A. *J. Am. Chem. Soc.* **2005**, *127*, 8408–8415.
(34) An, Y.; Tong, M.-L.; Ji, L.-N.; Mao, Z.-W. *Dalton Trans.* **2006**, 2066–2071.
(35) Corneillie, T. M.; Whetstone, P. A.; Lee, K. C.; Wong, J. P.; Meares, C. F. *Bioconjugate Chem.* **2004**, *15*, 1389–1391.
(36) Qian, J.; Gu, W.; Liu, H.; Gao, F.; Feng, L.; Yan, S.; Liao, D.; Cheng, P. *Dalton Trans.* **2007**, 1060–1066.
(37) Li, J.-H.; Wang, J.-T.; Zhang, L.-Y.; Chen, Z.-N.; Mao, Z.-W.; Ji, L.-N. *Inorg. Chim. Acta* **2009**, *362*, 1918–1924.
(38) Li, J.-H.; Wang, J.-T.; Hu, P.; Zhang, L.-Y.; Chen, Z.-N.; Mao, Z.-W.; Ji, L.-N. *Polyhedron* **2008**, *27*, 1898–1904.
(39) Kovari, E.; Heitker, J.; Kramer, R. *J. Chem. Soc. Chem. Commun.* **1995**, 1205–1206.
(40) Kovari, E.; Kramer, R. *J. Am. Chem. Soc.* **1996**, *118*, 12704–12709.
(41) Wall, M.; Linkletter, B.; Williams, D.; Lebuis, A.-M.; Hynes, R. C.; Chin, J. *J. Am. Chem. Soc.* **1999**, *121*, 4710–4711.
(42) Sheng, X.; Guo, X.; Lu, M.-X.; Lu, G., -Y.; Shao, Y.; Liu, F.; Xu, Q. *Bioconjugate Chem.* **2008**, *19*, 490–498.
(43) Kim, J. H.; Youn, M. R.; Lee, Y.-A.; Kim, J. M.; Kim, S. K. *Bull. Korean Chem. Soc.* **2007**, *28*, 263–270.
(44) Iranzo, O.; Elmer, T.; Richard, J. P.; Morrow, J. R. *Inorg. Chem.* **2003**, *42*, 7737–7746.
(45) Zhao, Y. M.; Zhu, J. H.; He, W. J.; Yang, Z.; Zhu, Y. G.; Li, Y. Z.; Zhang, J. F.; Guo, Z. J. *Chem.—Eur. J.* **2006**, *12*, 6621–6629.
(46) Wahnon, D.; Hynes, R. C.; Chin, J. *J. Chem. Soc. Chem. Commun.* **1994**, 1441–1442.
(47) Belousoff, M. J.; Tjioe, L.; Graham, B.; Spiccia, L. *Inorg. Chem.* **2008**, *47*, 8641–8651.
(48) Jubian, V.; Dixon, R. P.; Hamilton, A. D. *J. Am. Chem. Soc.* **1992**, *114*, 1120–1121.
(49) Dixon, R. P.; Geib, S. J.; Hamilton, A. D. *J. Am. Chem. Soc.* **1992**, *114*, 365–366.
(50) Jubian, V.; Veronese, A.; Dixon, R. P.; Hamilton, A. D. *Angew. Chem., Int. Ed.* **1995**, *34*, 1237–1239.
(51) Muche, M.-S.; Goebel, M. W. *Angew. Chem., Int. Ed.* **1996**, *35*, 2126–2129.
(52) Ariga, K.; Ansyln, E. V. *J. Org. Chem.* **1992**, *57*, 417–419.
(53) Ait-Haddou, H.; Sumaoka, J.; Wiskur, S. J.; Folmer-Andersen, J. F.; Ansyln, E. V. *Angew. Chem., Int. Ed.* **2002**, *41*, 4013–4016.
(54) Feng, G.; Mareque-Rivas, J. C.; de-Rosales, R. T. M.; Williams, N. H. *J. Am. Chem. Soc.* **2005**, *127*, 13470–13471.
(55) Feng, G.; Mareque-Rivas, J. C.; Williams, N. H. *Chem. Commun.* **2006**, 1845–1847.
(56) Chen, X. Q.; Wang, J. Y.; Sun, S. G.; Fan, J. L.; Wu, S.; Liu, J. F.; Ma, S. J.; Zhang, L. Z.; Peng, X. J. *Bioorg. Med. Chem. Lett.* **2008**, *18*, 109–113.
(57) He, J.; Hu, P.; Wang, Y. J.; Tong, M.-L.; Sun, H. Z.; Mao, Z.-W.; Ji, L.-N. *Dalton Trans.* **2008**, 3207–3214.
(58) Sheng, X.; Lu, X. M.; Chen, Y. T.; Lu, G., -Y.; Zhang, J. J.; Shao, Y.; Liu, F.; Xu, Q. *Chem.—Eur. J.* **2007**, *13*, 9703–9712.
(59) Shao, Y.; Sheng, X.; Li, Y.; Jia, Z. L.; Zhang, J. J.; Liu, F.; Lu, G. -Y. *Bioconjugate Chem.* **2008**, *19*, 1840–1848.

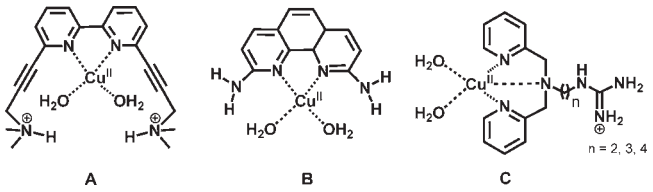

Figure 1. Examples of metal-based synthetic nucleases.

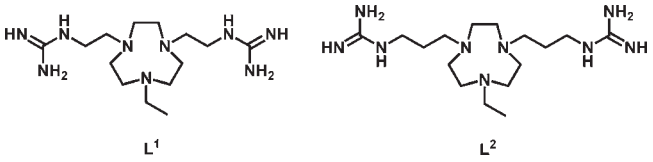

Figure 2. Ligands, $\mathbf{L^1}$ and $\mathbf{L^2}$, prepared in this study as tetrahydrochloride salts.

DPA ligands bearing guanidinium pendants of varying lengths (Figure 1C).[47] Again, the combination of a copper(II) center and guanidinium group in close proximity was found to result in an enhanced ability to cleave plasmid DNA and, in some cases, an RNA mimic (UpNP).

In this paper, we report the synthesis and cleavage properties of two further copper(II)-based synthetic nucleases featuring in-built cationic hydrogen-bond donors. The ligands used in this study are based on the well-known tacn macrocycle. Pioneering work by Burstyn and co-workers demonstrated that the copper(II) complex of tacn itself is capable of cleaving simple activated phosphate esters, DNA, RNA and peptides.[6] Building on this seminal study, a number of research groups, including our own, have shown that *N*-functionalization of tacn with various groups can enhance cleavage activity.[36,42−44] Here, we have prepared two new tacn-based ligands featuring pairs of guanidinium pendants, $\mathbf{L^1}$ and $\mathbf{L^2}$ (Figure 2), determined the crystal structure of the copper(II) complex of $\mathbf{L^1}$, and studied the solution speciation of the two complexes. The kinetics of cleavage of three different phosphate diesters, namely pBR 322 plasmid DNA, *bis*(*p*-nitrophenyl)phosphate (BNPP) and 2-hydroxypropyl-*p*-nitrophenyl phosphate (HPNPP), by the two complexes have also been investigated to gain some insight into the effect of the appended positively charged guanidinium groups on cleavage activity.

Experimental Section

Materials and Chemicals. Chemicals and solvents were of reagent or analytical grade, and were used as received unless otherwise indicated. Distilled H_2O and HPLC grade chloroform were used throughout. THF was dried over 4 Å molecular sieves and then freshly distilled from Na/benzophenone prior to use. 1,4-*bis*(*tert*-butoxycarbonyl)-1,4,7-triazacyclononane[60] and the sodium salt of 2-hydroxypropyl-*p*-nitrophenylphosphate (NaHPNPP)[61,62] were synthesized according to literature procedures. pBR 322 plasmid DNA was purchased from Promega Corporation. Milli-Q water used for DNA cleavage was sterilized by autoclaving and all reaction solutions were prepared according to standard sterile techniques. Deoxygenated water was prepared by boiling distilled water under nitrogen for 4 h and cooling while bubbling with nitrogen gas.

Instrumentation and Methods. Infrared spectra were recorded as KBr disks using a Bruker Equinox FTIR spectrometer fitted with an ATR platform at 4.0 cm^{-1} resolution. Microanalyses were performed by the Campbell Microanalytical Service, Otago, New Zealand. ^1H and ^{13}C NMR spectra were recorded at 25 °C in D_2O or $CDCl_3$ (as listed) on a Bruker AC200, AM300 or DX400 spectrometer. The chemical shifts, δ, were recorded on the δ scale in parts per million (ppm) and were calibrated using either tetramethylsilane (TMS) or signals because of the residual protons of deuterated solvents. Abbreviations used to describe ^1H NMR resonances are s (singlet), d (doublet), t (triplet), q (quartet), m (multiplet), and br s (broad singlet). Low-resolution electrospray ionization mass spectra (ESI-MS) were obtained with a Micromass Platform II Quadrupole Mass Spectrometer fitted with an electrospray source. The capillary voltage was set at 3.5 eV and the cone voltage at 35 V. Thin Layer Chromatography (TLC) was performed using silica gel 60 F-254 (Merck) plates with detection of species present by UV irradiation or $KMnO_4$ oxidation. UV−vis spectra were recorded in 1 cm quartz cuvettes using Varian Cary Bio 300 or 5G spectrophotometers. Agarose gel electrophoresis of plasmid DNA cleavage products was performed using a Biorad Mini-Protean 3 Electrophoresis Module. Bands were visualized by UV light irradiation, fluorescence imaged using an AlphaImager, and photographed with a CCD camera. The gel photographs were analyzed with the aid of the program ImageQuaNT version 4.1. Intensity values for supercoiled pBR 322 DNA were corrected by a factor of 1.42 to account for the decreased ability of ethidium bromide to intercalate into supercoiled DNA (Form I) compared to nicked DNA (Form II).[34] The relative proportions of each different form of DNA were determined by dividing the fluorescence intensity of each band by the sum of fluorescence intensities of all bands in the same lane. Background fluorescence was determined by reference to a lane containing no DNA.

Caution: *Although no problems were encountered in this work, perchlorate salts are potentially explosive. They should be prepared in small quantities and handled with care.*

Syntheses. Ethyl-4,7-bis(*tert*-butoxycarbonyl)-1,4,7-triazacyclononane (1). A solution of iodoethane (1.04 g, 6.68 mmol) in acetonitrile (50 mL) was added dropwise to a mixture of 1,4-bis(*tert*-butoxycarbonyl)-1,4,7-triazacyclononane (2.20 g, 6.68 mmol), K_2CO_3 (0.92 g, 13.4 mmol), and KI (0.12 g, 0.60 mmol) in acetonitrile (50 mL) and the resulting mixture stirred for 1 h at room temperature, then refluxed overnight. After cooling to room temperature, the inorganic salts were filtered off and the solvent removed from the filtrate under reduced pressure to yield **1** as a yellow oil. Yield: 2.01 g (84%). ^1H NMR (300 MHz, $CDCl_3$): δ 1.00 (t, 3H, $J = 7.2$ Hz, ethyl CH_3), 1.47 (s, 18H, ^{t}Bu CH_3), 2.58 (m, 6H, ethyl CH_2 and tacn ring CH_2), 3.25 (m, 4H, tacn ring CH_2), 3.47 (m, 4H, tacn ring CH_2). ^{13}C NMR (75 MHz, $CDCl_3$): δ 12.6 (ethyl CH_3), 28.3 (^{t}Bu CH_3), 49.6, 49.8 (tacn CH_2), 50.1, 50.6 (tacn CH_2), 52.7 (ethyl CH_2), 53.0, 53.2 (tacn CH_2), 79.0 (quaternary ^{t}Bu C), 155.4 (C=O). IR (neat), υ(cm^{-1}) 2973s (υ_{C-H}), 2932s (υ_{C-H}), 1694s ($\upsilon_{C=O}$), 1462s, 1413s, 1365s (υ_{C-O}), 1250s, 1175s, 988 m, 860 m, 773 m, 733 m. ESI-MS (m/z): 358.2 (100%) $[M + H]^+$.

1-Ethyl-1,4,7-triazacyclononane (2). Compound **1** (1.02 g, 2.86 mmol) was dissolved in a 1:1 v/v mixture of trifluoroacetic acid (TFA)/CH_2Cl_2 and the solution was stirred at room temperature overnight. The pH was then slowly adjusted to 14 by the careful addition of 5 M NaOH and the product extracted with CH_2Cl_2 (3 × 100 mL). The combined organic fractions were dried over $MgSO_4$, and following filtration, the solvent was removed under reduced pressure to yield **2** as a yellow oil. Yield: 0.39 g (85%). ^1H NMR (300 MHz, $CDCl_3$): δ 1.05 (t, 3H, $J =$ 7.2 Hz, ethyl CH_3), 2.59−2.70 (m, 6H, ethyl CH_2 and tacn ring CH_2), 2.78−2.85 (m, 8H, tacn ring CH_2), 3.15 (s br, 2H, NH). ^{13}C NMR (75 MHz, $CDCl_3$): δ 12.6 (ethyl CH_3), 45.6 (ethyl CH_2), 46.2 (tacn CH_2), 50.7 (tacn CH_2), 51.4 (tacn CH_2).

(60) Kimura, S.; Bill, E.; Bothe, E.; Weyhermuller, T.; Wieghardt, K. *J. Am. Chem. Soc.* **2001**, *123*, 6025–6039.
(61) Brown, D. M.; Usher, D. A. *J. Chem. Soc.* **1965**, 6558–6564.
(62) Tsang, J. S.; Neverov, A. A.; Brown, R. S. *J. Am. Chem. Soc.* **2003**, *125*, 1559–1566.

IR (neat), $\upsilon(cm^{-1})$ 3312 m br (υ_{N-H}), 1199 m (υ_{C-N}), 1078 m, 729 m. ESI-MS (m/z): 158.0 (100%) $[M + H]^+$.

1-Ethyl-4,7-bis(*tert*-butoxycarbonyl ethyl carbamate)-1,4,7-triazacyclononane (3). A solution of *tert*-butyl-(2-bromoethyl)-carbamate (1.90 g, 8.49 mmol) in acetonitrile (30 mL) was added dropwise to a mixture of **2** (0.67 g, 4.24 mmol), K_2CO_3 (1.46 g, 10.6 mmol) and KI (0.12 g, 0.60 mmol) in acetonitrile (30 mL). The mixture was stirred for 1 h at room temperature and then refluxed for 3 days. After the mixture was cooled to room temperature, the inorganic salts were removed by filtration. Evaporation of the solvent from the filtrate in vacuo yielded **3** as a yellow oil. Yield: 1.42 g (76%). ^{1}H NMR (300 MHz, $CDCl_3$): δ 1.02 (t, 3H, J = 7.2 Hz, ethyl CH_3), 1.46 (s, 18H, ^{t}Bu CH_3), 2.52−2.68 (m, 18H, tacn CH_2 and ethyl CH_2), 3.17 (m, 4H, ethyl CH_2), 5.29 (s br, 2H, NH). ^{13}C NMR (75 MHz, $CDCl_3$): δ 12.4 (ethyl CH_3), 28.2 (^{t}Bu CH_3), 38.7 (ethyl CH_2), 52.3, 54.6 (tacn CH_2), 56.7 (ethyl CH_2), 56.9 (ethyl CH_2), 57.2 (tacn CH_2), 78.3 (quaternary ^{t}Bu C), 155.9 (C=O). IR (neat), $\upsilon(cm^{-1})$ 3354s br (υ_{N-H}), 2977s (υ_{C-H}), 2933s (υ_{C-H}), 1684s ($\upsilon_{C=O}$), 1455s, 1251s (υ_{C-O}), 1170s, 922s, 732s. ESI-MS (m/z): 444.5 (100%) $[M + H]^+$.

1-Ethyl-4,7-bis(*tert*-butoxycarbonyl propyl carbamate)-1,4,7-triazacyclononane (4). Compound **4** was synthesized following the same procedure as for **3**, using **2** (0.76 g, 4.83 mmol), *tert*-butyl-(3-bromopropyl)carbamate (2.30 g, 9.65 mmol), K_2CO_3 (1.67 g, 12.1 mmol) and KI (0.11 g, 0.60 mmol). Yield: 1.98 g (88%). ^{1}H NMR (300 MHz, $CDCl_3$): δ 1.05 (t, 3H, J = 7.2 Hz, ethyl CH_3), 1.46 (s, 18H, ^{t}Bu CH_3), 1.50 (m, 4H, propyl CH_2), 2.45 (m, 6H, propyl CH_2 and ethyl CH_2), 2.58 (m, 12H, tacn CH_2), 3.05 (m, 4H, propyl CH_2), 3.25 (m, 2H, NH). ^{13}C NMR (75 MHz, $CDCl_3$): δ 12.4 (ethyl CH_3), 27.8 (propyl CH_2), 28.2 (^{t}Bu CH_3), 39.5 (propyl CH_2), 41.2 (ethyl CH_2), 52.1 (propyl CH_2), 55.2, 55.9, 57.1 (tacn CH_2), 78.4 (quaternary ^{t}Bu C), 160 (C=O). IR (neat), $\upsilon(cm^{-1})$ 3335s (υ_{N-H}), 2932s (υ_{C-H}), 2808s, 1694s ($\upsilon_{C=O}$), 1520s, 1391s, 1252s(υ_{C-O}), 1171s, 922w, 732s. ESI-MS (m/z): 472.4 (100%) $[M + H]^+$.

1-Ethyl-4,7-bis(2-aminoethyl)-1,4,7-triazacyclononane (5). A solution of the Boc-protected amine **3** (0.57 g, 1.29 mmol) was dissolved in a 1:1 v/v mixture of TFA/CH_2Cl_2 and the solution left stirring at room temperature overnight. Following adjustment of the pH to 14 by the cautious addition of 5 M NaOH, the product was extracted with CH_2Cl_2 (3 × 100 mL). Workup as for **2** gave **6** as a yellow oil. Yield: 0.28 g (88%). ^{1}H NMR (300 MHz, $CDCl_3$): δ 1.04 (t, 3H, J = 7.2 Hz, ethyl CH_3), 2.61 (m, 16H, tacn CH_2 and ethyl CH_2), 2.80 (m, 6H, ethyl CH_2). ^{13}C NMR (75 MHz, $CDCl_3$): δ 9.74 (ethyl CH_3), 37.7 (ethyl CH_2), 52.4 (ethyl CH_2), 52.9 (tacn CH_2), 53.2 (tacn CH_2), 54.8 (ethyl CH_2). IR (neat), $\upsilon(cm^{-1})$ 3003w (υ_{N-H}), 2975s (υ_{C-H}), 2932s (υ_{C-H}), 1432 m, 1182s, 799s. ESI-MS (m/z): 244.2 (100%) $[M + H]^+$.

1-Ethyl-4,7-bis(3-aminopropyl)-1,4,7-triazacyclononane (6). Compound **6** was synthesized from **4** (0.48 g, 1.01 mmol) following the same procedure as for **5**. This yielded the desired product as a brown oil. Yield: 0.21 g (75%). ^{1}H NMR (300 MHz, $CDCl_3$): δ 1.02 (t, 3H, J = 7.2 Hz, ethyl CH_3), 1.62 (m, 6H, propyl CH_2 and ethyl CH_2), 2.51−2.60 (m, 8H, propyl CH_2), 2.70−2.78 (m, 12H, tacn CH_2). ^{13}C NMR (75 MHz, $CDCl_3$): δ 11.7 (ethyl CH_3), 29.6 (propyl CH_2), 40.0 (propyl CH_2), 51.5 (ethyl CH_2), 53.2 (propyl CH_2), 53.9, 56.4, 66.7 (tacn CH_2). IR (neat), $\upsilon(cm^{-1})$ 3334s (υ_{N-H}), 2930s (υ_{C-H}), 1463 m, 1173s, 1128s, 923w, 731s. ESI-MS (m/z): 271 (100%) $[M + H]^+$.

1-Ethyl-4,7-bis[2-bis(*tert*-butoxycarbonyl)guanidinoethyl]-1,4,7-triazacyclononane (7). To a stirred solution of **5** (0.57 g, 2.35 mmol) in THF (20 mL) was added a solution of *N*,*N*′-Boc$_2$-1*H*-pyrazole-1-carboxamidine (1.47 g, 4.71 mmol) in THF (20 mL). The resulting solution was stirred under nitrogen at room temperature for 2 days. The solvent was then evaporated under reduced pressure, and the residue taken up in DCM (50 mL). After it was washed with 0.1 M NaOH (3 × 30 mL), the organic fraction was dried over Na_2SO_4 and the solvent removed under reduced pressure to yield crude **7** as a yellow oil. The crude product was purified by column chromatography (Merck neutral alumina gel 90, eluent: 2% MeOH/$CHCl_3$), with the desired fraction having an R_f = 0.35. Yield: 0.95 g (55%). ^{1}H NMR (300 MHz, $CDCl_3$): δ 1.02 (t, 3H, J = 7.2 Hz, ethyl CH_3), 1.49 (s, 36H, ^{t}Bu CH_3), 2.55 (m, 4H, ethyl CH_2), 2.65−2.79 (m, 14H, tacn CH_2 and ethyl CH_2), 3.47 (m, 4H, ethyl CH_2). ^{13}C NMR (75 MHz, $CDCl_3$): δ 12.7 (ethyl CH_3), 27.4, 28.0 (^{t}Bu CH_3), 39.1 (ethyl CH_2), 51.2 (ethyl CH_2), 54.3 (ethyl CH_2), 55.6, 56.1, 57.1 (tacn CH_2), 78.6, 82.3 (quaternary ^{t}Bu C), 152.5 (C=O), 155.7 (C=O), 163.3 (C=N). IR (neat), $\upsilon(cm^{-1})$ 3331s (υ_{N-H}), 2976s (υ_{C-H}), 1732s ($\upsilon_{C=O}$), 1651s ($\upsilon_{C=N}$), 1557s, 1416s, 1167s (υ_{C-O}), 1057s, 1026s, 913 m. ESI-MS (m/z): 728.5 (100%) $[M + H]^+$.

1-Ethyl-4,7-bis[3-bis(*tert*-butoxycarbonyl)guanidinopropyl]-1,4,7-triazacyclononane (8). Compound **8** was prepared using the same method as for **7** by dissolving compound **6** (0.54 g, 1.99 mmol) in THF (20 mL), followed by the addition of *N*,*N*′-Boc$_2$-1*H*-pyrazole-1-carboxamidine (1.23 g, 3.98 mmol) in THF (20 mL). The desired product has an R_f = 0.32. Yield: 0.85 g (57%). ^{1}H NMR (300 MHz, $CDCl_3$): δ 0.98 (m br, 2H, NH), 1.00 (t, 3H, J = 7.2 Hz, ethyl CH_3), 1.25 (m, 6H, propyl CH_2 and ethyl CH_2), 1.47 (s, 36H, ^{t}Bu CH_3), 1.72 (m, 4H, propyl CH_2), 2.50−2.60 (m, 12H, tacn CH_2), 3.47 (m, 4H, propyl CH_2), 8.34 (t br, 2H, NHBoc). ^{13}C NMR (75 MHz, $CDCl_3$): δ 12.8 (ethyl CH_3), 27.4, 28.0 (^{t}Bu CH_3), 28.3, 29.6 (propyl CH_2), 39.2 (ethyl CH_2), 52.2, 55.0, 56.1 (tacn CH_2), 79.0, 82.9 (quaternary ^{t}Bu C), 153.2 (C=O), 156.1 (C=O), 163.6 (C=N). IR (neat), $\upsilon(cm^{-1})$ 3334s (υ_{N-H}), 2934s (υ_{C-H}), 1715s ($\upsilon_{C=O}$), 1644s ($\upsilon_{C=N}$), 1555s, 1455s, 1252s (υ_{C-O}), 1133s, 1048s, 913 m. ESI-MS (m/z): 756.3 (100%) $[M + H]^+$.

1-Ethyl-4,7-bis(ethylguanidinium)-1,4,7-triazacyclononane tetrahydrochloride ($L^1 \cdot 4HCl$). A solution of the Boc-protected amine **7** (0.68 g, 0.93 mmol) was dissolved in a 1:1 v/v mixture of TFA/CH_2Cl_2 and the solution stirred at room temperature overnight. The solvent was then removed under reduced pressure and the residual brown oil taken up in a mixture of EtOH (5 mL) and concentrated HCl (2 mL). Addition of Et_2O (5 mL) produced a pale yellow precipitate, which was collected by filtration, dissolved in a small volume of water and then freeze-dried to yield the product as a yellow solid. Yield: 0.23 g (75%). Microanalysis: Calcd for $C_{14}H_{33}N_9Cl_4$ C 33.0, H 8.1, N 24.8, Cl 27.9%; Found C 33.3, H 8.1, N 24.3, Cl 27.6%. ^{1}H NMR (300 MHz, D_2O): δ 1.50 (t, 3H, J = 7.2 Hz, ethyl CH_3), 2.96 (m, 4H, tacn CH_2), 3.13 (m, 8H, tacn CH_2), 3.43 (m, 6H, ethyl CH_2), 3.51 (m, 4H, ethyl CH_2). ^{13}C NMR (75 MHz, D_2O): δ 9.30 (ethyl CH_3), 37.1 (ethyl CH_2), 49.2, 49.6, 50.1 (tacn CH_2), 54.3 (ethyl CH_2), 55.4 (ethyl CH_2) 157.7 (C=N). IR (KBr disk), $\upsilon(cm^{-1})$: 3404s (υ_{N-H}), 2977s (υ_{C-H}), 2960s (υ_{C-H}), 1664s ($\upsilon_{C=N}$), 1450 m, 1230w, 1178w, 940w. ESI-MS (m/z): 164.7 (90%) $[M + 2H]^{2+}$, 328.4 (10%) $[M + H]^+$.

1-Ethyl-4,7-bis(propylguanidinium)-1,4,7-triazacyclononane tetrahydrochloride ($L^2 \cdot 4HCl$). Deprotection of compound **8** (0.57 g, 0.90 mmol) was carried out in the same fashion as for compound **7** to yield the product as a yellow solid. Yield: 0.16 g (78%). Microanalysis: Calcd for $C_{16}H_{37}N_9Cl_4$ C 36.4, H 8.3, N 23.9, Cl 26.9%; Found C 36.4, H 8.2, N 24.0, Cl 27.1%. ^{1}H NMR (300 MHz, D_2O): δ 1.47 (t, 3H, J = 7.2 Hz, ethyl CH_3), 1.97 (m, 4H, propyl CH_2), 3.08 (m, 4H, tacn CH_2), 3.23 (m, 8H, tacn CH_2), 3.37 (m, 6H, propyl CH_2 and ethyl CH_2), 3.53 (m, 4H, propyl CH_2). ^{13}C NMR (75 MHz, D_2O): δ 9.43 (ethyl CH_3), 23.6 (propyl CH_2), 39.0 (propyl CH_2), 49.1 (ethyl CH_2), 49.3 (propyl CH_2), 50.0, 53.9, 54.1 (tacn CH_2), 157.2 (C=N). IR (KBr disk), $\upsilon(cm^{-1})$: 3412s (υ_{N-H}), 2954s (υ_{C-H}), 1668s ($\upsilon_{C=N}$), 1436 m, 1172w, 1018w. ESI-MS (m/z): 356.4 (100%) $[M + H]^+$.

$[CuL^1](ClO_4)_2$ (C1). To a stirred solution of L^1.4HCl (0.093 g, 0.18 mmol) in water (4 mL) was added a solution of Cu(ClO_4)$_2$.6H_2O (0.081 g, 0.22 mmol) in water (4 mL). The pH of the solution was adjusted to 9 with 1 M NaOH, resulting in a

color change to deep blue. An off-white precipitate of $Cu(OH)_2$ was removed by filtration, and the deep blue solution left to slowly evaporate in a crystallization dish, resulting in the formation of blue crystals of the product. Yield: 0.043 g (41%). Microanalysis: Calc for $Cu_1C_{14}H_{33}N_9O_8Cl_2$: C 28.5, H 5.6, N 21.4%, Found: C 28.2, H 5.7, N 21.4%. UV−vis (H_2O): λ_{max} (nm) [ε_{max}] (M^{-1} cm^{-1}): 600 [250], 750 [85], 985 [125]. Selected IR bands (ATR) υ(cm^{-1}): 3445 m, 3348 m, 3252 m (υ_{N-H}), 2967w, 2862w (υ_{C-H}), 1584s ($\upsilon_{C=N}$), 1031s br, 618s (υ_{ClO4}^-).

Solution Speciation Studies. pH titrations of C1 and C2. pH titrations were carried out by adding 1 μL aliquots of 10 M HCl to solutions of the Cu(II) complexes ([**C1**] = 9.28 mM, [**C2**] = 7.2 mM, total volume 10 mL). Stock copper(II) complexes solutions were prepared by mixing equimolar amounts of the desired ligands and $CuCl_2.2H_2O$ in water. The solutions were stirred for 1 min after each addition to ensure that the pH was stable, and then the background-corrected UV−vis-NIR spectrum measured.

The series of spectra were analyzed using the BEEROZ software.[63] Briefly, this method employs constrains from mass balance and mass action equations in order to test speciation models for spectral data sets containing many species, and to derive formation constants for the spectroscopically active species.[64,65] The analysis provides the calculated spectra based on the model, the spectra for the individual complexes, and formation constants for all species included in the model. For the present study, activity coefficients were fixed to unity (fixed ionic strength).

Titration of C1 with (4-Nitrophenyl)phosphate (NPP). Aliquots (1 μL) of a 1.39 M NPP solution were added to solutions of complex **C1** (9.28 mM, final volume 3 mL), buffered at pH 6.0, 7.0, and 9.0 with 1 M MES, HEPES and CHES, respectively. A background-corrected UV−vis-NIR spectrum was measured after each addition of NPP. The NPP binding constant, K_b, was be determined from the variation in absorbance with [NPP] by using the equation $(A - A_0)/[NPP] = -K_b(A - A_0) + K_b[CuL]_0(\varepsilon_{CuLNPP} - \varepsilon_{CuL})$, where A = absorbance at a particular [NPP], A_0 = initial absorbance, $[CuL]_0$ = initial copper(II) complex concentration, and ε_{CuL} and ε_{CuLNPP} = molar extinction coefficients for copper complex and complex with NPP bound, respectively. The plot of $(A - A_0)/[NPP]$ vs $(A - A_0)$ was found to be linear with the slope of the graph corresponding to the binding constant.

Cleavage of Model Phosphate Esters. Bis(*p*-nitrophenyl)phosphate (BNPP). These experiments were conducted using established procedures.[66,67] Briefly, the rate of cleavage of BNPP by the Cu(II) complexes was measured at pH 7.0 (HEPES buffer) and T = 50 °C, by following the formation of *p*-nitrophenoxide ion (λ_{max} = 400 nm, λ_{max} = 18,700 M^{-1} cm^{-1}) in solutions containing 0.1 mM BNPP, 2 mM Cu(II) complex and 0.15 M $NaClO_4$. Stock copper(II) complexes solutions were prepared by mixing equimolar amounts of the desired ligands and $CuCl_2 \cdot 2H_2O$ in water and adjusting the pH to 7 with addition of NaOH. Absorbance measurements were commenced 2 min after mixing and were continued for 8000 min, with a reading taken every 15 min. As the complex was in large excess compared to BNPP, the time dependence of the appearance of NP (and cleavage of BNPP) was modeled as a first-order process. Observed rate constants were determined by fitting the data to the equation, $Abs = A + Be^{-k_{obs}t}$, where A and B are constants, or by the initial rate method (i.e., directly from the plot of the increase of *p*-nitrophenolate concentration versus time). The latter gave linear plots with typical R^2 values > 0.995.[68]

2-Hydroxypropyl-*p*-nitrophenylphosphate (HPNPP). These experiments were carried out in a similar manner to the BNPP experiments. The rate of cleavage of HPNPP by the Cu(II) complexes was measured at pH 7.0 (HEPES buffer) and T = 25 °C, again by following the release of the highly colored *p*-nitrophenoxide ion (vide supra), in solutions containing 0.1 mM HPNPP, 2 mM Cu(II) complex, and 0.15 M $NaClO_4$. The observed rate constants were determined by fitting the data to the expression, $Abs = A + Be^{-k_{obs}t}$.

DNA Cleavage Experiments. Reaction mixtures (total volume 15 μL) containing pBR 322 supercoiled plasmid DNA (38 μM base pair concentration) and copper(II) complex (75, 100, 150, 300, and 600 μM) dissolved in 40 mM buffers (MES, HEPES, TAPS, and CHES) at pH 6.0, 6.5, 7.0, 7.5, 8.0 and 9.0, were incubated in a water bath at 37 °C for periods of up to 48 h. Loading buffer (0.1 M EDTA, 40% (w/v) sucrose, 0.05% (w/v) bromophenol blue, and 0.5% (w/v) sodium lauryl sulfate, SDS) (5 μL) was added to stop the reactions at defined time periods, and the resulting solutions stored at −20 °C until just prior to analysis. The solutions were then loaded onto 1% agarose gels containing 1.0 μg dm^{-3} ethidium bromide, and the DNA fragments separated by gel electrophoresis (70 V for 2 h in 1 x tris-acetate EDTA (TAE) buffer). Ethidium-stained agarose gels were imaged, and the extent of supercoiled DNA cleavage determined via densitometric analysis of the visualized bands using the volume quantification method. Experiments were performed at least in duplicate. The variation in the amount of DNA cleavage with time was modeled as a first-order process, $Abs = A + Be^{-k_{obs}t}$ and observed rate constants determined by fitting the decrease in the relative intensity of Form I band as well as the appearance of the Form II band to this expression.

DNA Cleavage Experiments in the Presence of Radical Scavengers. Aliquots (5 μL) of aqueous solutions of scavenging agents (30 mM KI, DMSO, ^{t}BuOH or NaN_3 in 40 mM HEPES buffer at pH 7.0) were added to the solutions of supercoiled DNA (5 μL, 113.5 μM base pair concentration) prior to the addition of complexes **C1** and **C2**. The final reaction conditions were 150 μM for copper(II) complexes, 10 mM concentration for the scavenging agents and 38 μM base pair concentration for supercoiled plasmid DNA. Each solution was incubated at 37 °C for 6 h, quenched and analyzed according the procedures described above.

DNA Cleavage under Anaerobic Condition. Experiments under anaerobic condition were performed following the protocol reported by Burstyn and co-workers.[14] Deoxygenated water was prepared by five freeze−pump−thaw cycles. Before each cycle the water was equilibrated by bubbling nitrogen through the solution. It was used immediately in the preparation of anaerobic stock solutions in a nitrogen-filled environment. Reaction mixtures were prepared immediately by addition of the appropriate amounts of stock solutions to reaction tubes, which were subsequently sealed and incubated at 37 °C. All other conditions were as for the cleavage experiments performed under aerobic condition in which final concentrations for the reaction mixtures were 150 μM for complexes, 40 mM HEPES buffer, and 38 μM base pair concentration for plasmid DNA.

X-ray Crystallography. Intensity data for a blue crystal of **C1** (0.20 × 0.20 × 0.05 mm) were collected at 123 K on a Bruker Apex II CCD fitted with graphite monochromated Mo Kα radiation (0.71073 Å). The data was collected to a maximum 2θ value of 55° and processed using Bruker Apex II software package. Crystal parameters and details of the data collection are summarized in Table S01 in Supporting Information. The structure of **C1** was solved using SHELX-97[69,70] and expanded using standard Fourier transform routines. All hydrogen atoms

(63) Brugger, J. *Comput. Geosci.* **2007**, *33*, 248–261.
(64) Brugger, J.; McPhail, D. C.; Black, J.; Spiccia, L. *Geochim. Cosmochim. Acta* **2001**, *65*, 2691–2708.
(65) Liu, W.; Etschmann, B.; Brugger, J.; Spiccia, L.; Foran, G.; McInnes, B. *Chem. Geol.* **2006**, *231*, 326–349.
(66) Fry, F.; Fischmann, A. J.; Belousoff, M. J.; Spiccia, L.; Brugger, J. *Inorg. Chem.* **2005**, *44*, 941–950.
(67) Belousoff, M. J.; Duriska, M. B.; Graham, B.; Batten, S. R.; Moubaraki, B.; Murray, K. S.; Spiccia, L. *Inorg. Chem.* **2006**, *47*, 3746–3755.
(68) Deal, K. A.; Burstyn, J. N. *Inorg. Chem.* **1996**, *35*, 2792–2798.
(69) Sheldrick, G. M. *SHELXL-97*; University of Göttingen: Göttingen, Germany, 1997.
(70) Sheldrick, G. M. *SHELXS-97*; University of Göttingen: Göttingen, Germany, 1997.

Scheme 1. Synthesis of Hydrochloride Salts of Ligands $\mathbf{L^1}$ and $\mathbf{L^2}$

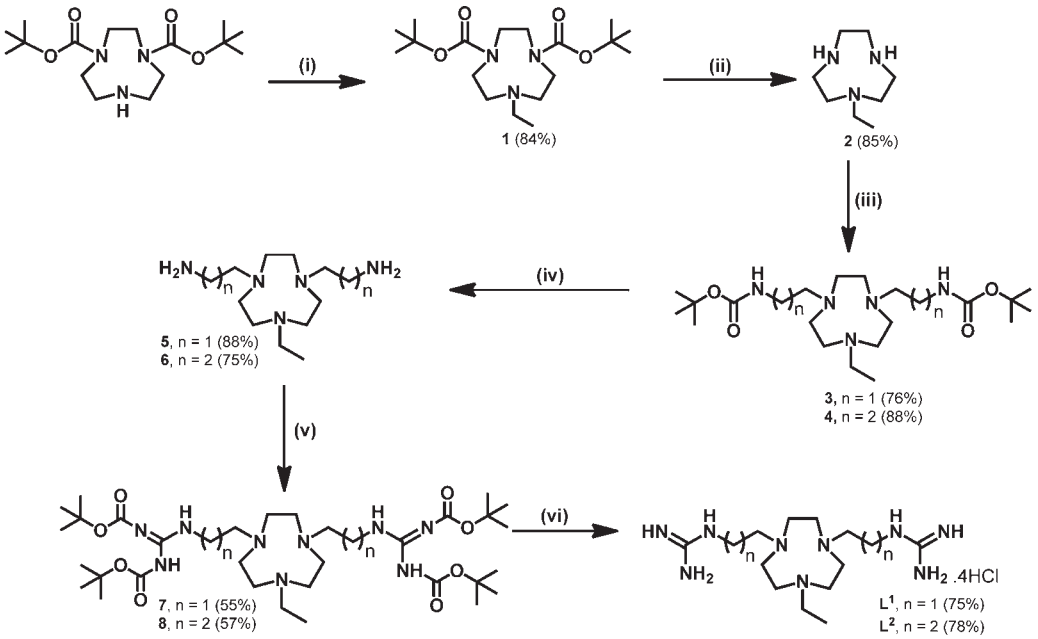

(i) iodoethane, K_2CO_3, CH_3CN, reflux, o/n; (ii) TFA/CH_2Cl_2 (1:1), RT, o/n; (iii) 2 *tert*-butyl(bromoalkyl)carbamate, K_2CO_3, KI (cat), CH_3CN, reflux, 3 days; (iv) TFA/CH_2Cl_2 (1:1), RT, o/n; (v) 2 equiv. *N,N'*-Boc_2-1*H*-pyrazole-1-carboxamidine, THF, RT, 2 days; (vi) a) TFA/CH_2Cl_2 (1:1), RT, o/n, b) Conc. HCl

were placed in idealized positions, except for the hydrogens on the nitrogen atoms, which were located on the Fourier difference map and refined with restrained N−H distances. The position of the N−H hydrogen atom, H8N, located as a Fourier difference peak, could not be modeled unambiguously, the hydrogen bonding interaction with the neighboring perchlorate anions present in the lattice ((N(8)−H(8N)···O(3)#3 = 3.160(7) Å, 148(5)°, #3 denoting the symmetry operator $(-x + 1, -y + 1, -z + 1)$, Table 3), as well as the differences in the corresponding guanidine C−N bond distances forming the basis for its assignment. The isotropic thermal parameters for N−H hydrogen atoms were fixed at 1.2 times that of the respective nitrogen atom. All non-hydrogen atoms were refined anisotropically.

Results and Discussion

Synthesis. The synthesis of the new tacn derivatives, $\mathbf{L^1}$ and $\mathbf{L^2}$, featuring pairs of guanidinium pendants followed the route shown in Scheme 1. This involved, first, reaction of 1,4-*bis*(*tert*-butoxycarbonyl)-1,4,7-triazacyclononane with iodoethane to alkylate one of the three nitrogens of the tacn ring. The Boc protecting groups were then removed through treatment with TFA, and guanidinium pendants introduced at the two exposed secondary nitrogens via a four-step procedure involving the addition of aminoalkyl pendants, followed by conversion of the terminal amino groups into guanidinium groups via treatment with *N,N'*-Boc_2-1*H*-pyrazole-1-carboxamidine. The new compounds were characterized by ^{1}H and ^{13}C NMR spectroscopy, ESI mass spectrometry, and IR spectroscopy. Satisfactory microanalyses were obtained for the final ligands, isolated as their tetrahydrochloride salts.

The copper(II) complex of $\mathbf{L^1}$, $[Cu\mathbf{L^1}](ClO_4)_2$ (**C1**), was isolated following slow evaporation of an aqueous solution of the ligand and $Cu(ClO_4)_2 \cdot 6H_2O$ adjusted to pH 9. Efforts to isolate **C2** were unsuccessful, probably because of the complexity of solution speciation (vide infra). Microanalytical data for **C1** were consistent with the proposed formula and the IR spectrum of the complex shows bands due to NH stretches of the guanidine groups in the region of 3252−3444 cm^{-1}, a sharp band at 1584 cm^{-1} attributed to the ν(C=N) of the guanidine groups, and bands at ~1031 and 618 cm^{-1} due to the perchlorate counterions. The electronic spectrum of **C1** exhibits bands at 600 and 985 nm, which are typical for a copper(II) complex with square pyramidal geometry. In addition, there is a band at 750 nm, which could arise from significant distortion of the Cu(II) coordination sphere, as identified in the X-ray structure determination (vide infra).

Crystallography. The complex **C1** crystallizes in the space group $P2_1/c$. The molecular structure consists of discrete five-coordinate $[Cu\mathbf{L^1}]^{2+}$ cations and noncoordinating perchlorate anions. A thermal ellipsoid representation of the complex cation is shown in Figure 3, while selected bond lengths and angles are listed in Table 1. The copper(II) coordination sphere is occupied by the three nitrogen atoms of the tacn ring and by a nitrogen donor from each of the guanidine groups, which are present in their neutral form. The guanidine groups bind via the nonterminal amine nitrogen, forming five-membered chelate rings. A search of the Cambridge Crystallography Database revealed that **C1** is the first example of a pendant guanidine group adopting this type of chelation mode. Binding of a guanidine group appended to a macrocycle has been previously reported by Kimura and coworkers,[71] for a zinc(II)-cyclen compound, however, in this case, binding was through one of the terminal amines and led to formation of a seven-membered chelate ring. Deprotonation and coordination of guanidine at near neutral pH was somewhat unexpected, given the strongly

(71) Aoki, S.; Iwaida, K.; Hanamoto, N.; Shiro, M.; Kimura, E. *J. Am. Chem. Soc.* **2002**, *124*, 5256–5257.

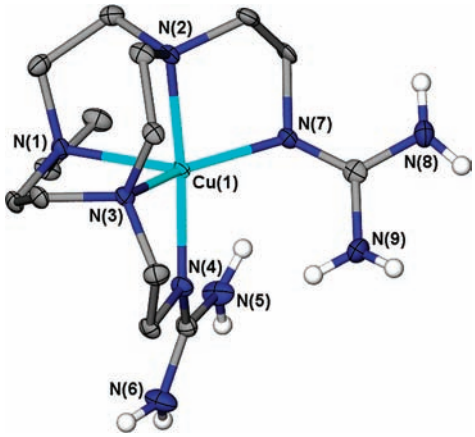

Figure 3. Thermal ellipsoid representation of the complex cation unit in **C1** (ellipsoids drawn at 50% probability; selected hydrogen atoms and perchlorate counterions are omitted for clarity).

Table 1. Selected Bond Lengths [Å] and Angles [deg] for **C1**

Cu(1)−N(1)	2.215(4)	N(7)−Cu(1)−N(4)	103.01(2)
Cu(1)−N(2)	2.067(4)	N(7)−Cu(1)−N(2)	85.2 (2)
Cu(1)−N(3)	2.092(4)	N(4)−Cu(1)−N(2)	168.0 (2)
Cu(1)−N(4)	2.001(4)	N(7)−Cu(1)−N(3)	136.7(2)
Cu(1)−N(7)	1.997(4)	N(4)−Cu(1)−N(3)	83.2 (2)
		N(2)−Cu(1)−N(3)	84.8(2)
		N(7)−Cu(1)−N(1)	136.4(2)
		N(4)−Cu(1)−N(1)	97.8(2)
		N(2)−Cu(1)−N(1)	81.5(2)
		N(3)−Cu(1)−N(1)	83.2(2)

basic character of guanidine (*viz*., guanidinium groups typically have pK_a values > 12[72]). The strength of binding to the copper(II) center clearly overrides the proton affinity of guanidine (see speciation studies). This can be attributed in part to the formation of five-membered chelate rings. The high affinity of the deprotonated guanidines for copper(II) is highlighted by the fact that the two Cu−N(pendant) distances are significantly shorter than those for the macrocyclic nitrogens, av. 1.999(4) Å vs 2.067(4)−2.215(4) Å.

The presence of five-membered chelate rings in the **C1** complex cation (in particular the three fused edge-sharing chelate rings of the tacn moiety) leads to considerable distortion from an idealized coordination geometry, with all intra-ring N−Cu−N angles well below 90° (Table 1). An effective means of quantifying the degree of distortion in five-coordinate copper(II) complexes was developed by Addison et al.,[73] which applies the parameter, τ, defined as $\{(\theta - \phi)/60\} \times 100$, where θ and ϕ are the largest and smallest basal angle, respectively (τ is zero for a square pyramidal geometry and one for a trigonal bipyramidal geometry). For **C1**, the relevant angles, $\theta = 168.0°$ and $\phi = 136.7°$, yield a τ value of 52%, which implies a Cu(II) geometry intermediate between the two regular extremes.

The guanidine groups of $\mathbf{L^1}$ are involved in weak hydrogen bonding interactions with the two non-coordinated perchlorate anions, leading to an extended intermolecular hydrogen bonding network within the crystal lattice of **C1** (see Figure 4 and Table 2).

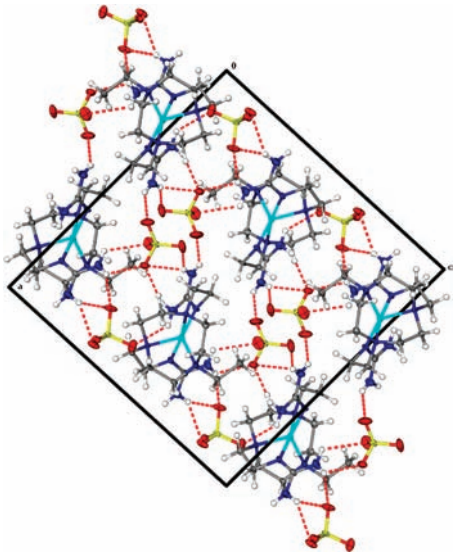

Figure 4. Hydrogen-bonding interactions (shown as dashed bonds) between the complex cation and the perchlorate anions present in the crystal lattice of **C1**, as viewed along the *b* axis.

Table 2. Hydrogen Bonding Interactions in **C1** [Å and deg][a]

D−H···A	*d*(D−H)	*d*(H···A)	*d*(D···A)	∠(DHA)
N(6)−H(2N)···O(6)	0.885(19)	2.47(4)	3.221(6)	143(5)
N(6)−H(2N)···O(7)	0.885(19)	2.30(3)	3.139(6)	159(5)
N(6)−H(1N)···O(8)#1	0.88(2)	2.25(2)	3.116(6)	171(5)
N(5)−H(3N)···O(7)	0.883(19)	2.51(3)	3.334(6)	155(5)
N(5)−H(3N)···O(1)	0.883(19)	2.52(4)	3.185(6)	132(5)
N(5)−H(4N)···O(4)	0.87(2)	2.48(5)	2.973(6)	116(4)
N(9)−H(5N)···O(5)#2	0.88(2)	2.60(5)	3.099(7)	117(4)
N(9)−H(6N)···O(1)#2	0.875(19)	2.51(3)	3.311(6)	152(5)
N(8)−H(7N)···O(2)#2	0.87(2)	2.31(3)	3.096(7)	149(5)
N(8)−H(7N)···O(1)#2	0.87(2)	2.57(3)	3.378(6)	153(5)
N(8)−H(8N)···O(3)#3	0.88(2)	2.38(3)	3.160(7)	148(5)

[a] Symmetry transformations used to generate equivalent atoms: #1 $-x, y+1/2, -z+1/2$; #2 $x, -y+1/2, z+1/2$; #3 $-x+1, -y+1, -z+1$.

In **C1**, the Cu−N bond lengths to the coordinating guanidine nitrogens are similar to those reported in the literature for other Cu(II)−tacn complexes bearing pendant amino arms with coordinating nitrogen atoms (av. *ca*. 2.0 Å, see Table 3). The Cu(1)−N(4) and Cu(1)−N(5) bonds in **C1** are virtually identical in length to the Cu−N(pendant) bond in $Cu[tacn(CH_2CH_2NH_2)]^{2+}$, where only one aminoethyl pendant coordinates to the copper(II) center. However, this bond distance is increased by *ca*. 0.02 Å in $Cu[tacn(CH_2CH_2NH_2)_2]^{2+}$, which features an additional coordinating aminoethyl pendant.[74] The Cu−N(pyridine) bond distances seen in Cu(II)-tacn complexes containing pyridyl pendants are also similar in size (1.99−2.02 Å).[75] Overall, this analysis is indicative of strong binding between the Cu(II) center and the guanidine groups in **C1**. This could be contributing to the high distortion of the copper(II) coordination sphere. The τ of 52% indicates that the degree of geometrical distortion is much greater than generally found for Cu(II)−tacn

(72) Riordan, J. F.; McElvany, K. D.; Borders, C. L. *Science* **1977**, *195*, 884–886.
(73) Addison, A. W.; Rao, T. N.; Reedjik, J.; Rijin, J. V.; Verschoor, G. C. *J. Chem. Soc., Dalton Trans*. **1984**, 1349–1356.
(74) Tei, L.; Bencini, A.; Blake, A. J.; Lippolis, V.; Perra, A.; Valtancoli, B.; Wilson, C.; Schroder, M. *Dalton Trans*. **2004**, 1934–1944.
(75) Gasser, G.; Tjioe, L.; Graham, B.; Belousoff, M. J.; Juran, S.; Walther, M.; Kunstler, J.-U.; Bergmann, R.; Stephan, H.; Spiccia, L. *Bioconjugate Chem*. **2008**, *19*, 719–730.

Table 3. Comparison of Selected Structural Parameters for **C1** with Those for Other Cu(II)−tacn Complexes Featuring Pendants with N Donors[a]

complex	$Cu-N_{(tacn)}$ (axial) (Å)	$Cu-N_{(tacn)}$ (equat.) (Å)	$Cu-N_{(pendant)}$ (Å)	τ (%)	chelate ring	refs
C1	2.215(4)	2.067(4); 2.092(4)	1.997(4); 2.001(4)	52	5	this work
$Cu(dmptacn)^{2+}$	2.162(8)	2.071(8); 2.000(8)	2.015(8); 2.016(8)	32	5	76
$Cu_2(tmpdtne)^{2+}$	2.205(4)	1.978(4); 2.009(4)	1.993(4); 2.001(4)	11	5	76
$Cu[tacn(CH_2CH_2NH_2)]^{2+}$	2.119(10)	2.100(9); 2.119(10)	1.995(9)	3	5	74
$Cu[tacn(CH_2CH_2NH_2)_2]^{2+}$,	2.206(2)	2.054(2); 2.033(2)	2.018(3); 2.019(3)	19	5	74
$Cu[^{i}Prtacn(CH_2CH_2CH_2NH_2)_2]^{2+}$	2.356(3)	2.062(4); 2.082(4)	2.032(3); 2.039(3)	20	6	77
$Cu[Bn^{i}Prtacn(CH_2CH_2CH_2NH_2)]^{2+}$	2.215(2)	2.026(2); 2.075(2)	2.008(2)	18	6	77

[a] Abbreviations: dmptacn = 2-[4,7-bis(2-pyridylmethyl)-1,4,7-triazacyclononane; tmpdtne = 1,2-*bis*[*N*,*N*′-bis(2-pyridylmethyl)-1,4,7-triazacyclononyl]ethane; $tacn(CH_2CH_2NH_2)$ = 1-(2-aminoethyl)-1,4,7-triazacyclononane,; $tacn(CH_2CH_2NH_2)_2$ = 1,4-bis(2-aminoethyl)-1,4,7-triazacyclononane; $^{i}Prtacn(CH_2CH_2CH_2NH_2)_2$ = 1,4-bis(3-aminopropyl)-7-isopropyl-1,4,7-triazacyclononane; $Bn^{i}Prtacn(CH_2CH_2CH_2NH_2)$ = 1-(3-aminopropyl)-4-benzyl-7-isopropyl-1,4,7-triazacyclononane.

complexes with pendant coordinating groups (range of 3−32%, Table 3), whose geometry is closer to square pyramidal.

Solution Speciation Studies. Spectrophotometric pH Titrations. To investigate the solution speciation of complexes **C1** and **C2**, a series of spectrophotometric pH titrations were performed, which monitored changes in the electronic spectrum of each complex as a function of pH (Figures 5 and 6). The titrations were commenced at pH ∼12 and spectra were measured after addition of aliquots of acid. In the case of **C1**, the complex with both guanidine pendants coordinated (**C1**) was anticipated to be the only species at pH 12, given that this complex crystallizes from solution at pH 9. This was confirmed by the fact that the UV−vis spectra remained constant over the pH range 8−12 (Figure 5b). As the pH decreased, major changes in spectrum were observed below pH 8, the most significant being the loss of the peak at ∼750 nm, but the peaks at ∼600 and 985 nm also shifted to ∼670 and 1050 nm. These changes in spectrum can be attributed to a shift to a more ideal square pyramidal geometry and a weakening of the ligand field around the copper(II) center, most likely arising from protonation of the coordinated guanidines and displacement from the coordination sphere by water, namely, CuN_5 is converted to CuN_3O_2. Principal component analysis (PCA) revealed that three species are required to describe the spectral changes with pH (Figure S01 in Supporting Information), and a model based on two successive protonation processes was successfully used to fit the data, from which apparent binding constants (K_{app1} and K_{app2}) could be determined, corresponding to deprotonation of each guanidinium group and coordination of the resultant guanidine (Scheme 2).

The pK_{app1} and pK_{app2} values were found to be 3.98 and 5.72, respectively (Figure 5c). This speciation model provides an extremely good fit to the data, with a maximum difference of ±0.012 absorbance units between the experimental and calculated data. In a study of the zinc(II) complex of a cyclen monoguanidinium derivative, Kimura and co-workers[71] were unable to determine the pK_a of the pendant guanidium group from pH titrations on the ligand in the absence of Zn^{2+} (but estimated it to be >12), yet the apparent binding constant for deprotonation/coordination of the guanidine groups was determined to be 5.9. This implies a remarkable binding affinity of zinc(II) for the guanidine group (log K > 6), even though a seven-membered chelate involving the terminal nitrogen was formed. In our case, an even higher binding affinity is apparent (log K > 6.5), which probably arises from the formation of more stable five-membered chelate rings involving the nonterminal amine nitrogen of the guanidine groups.

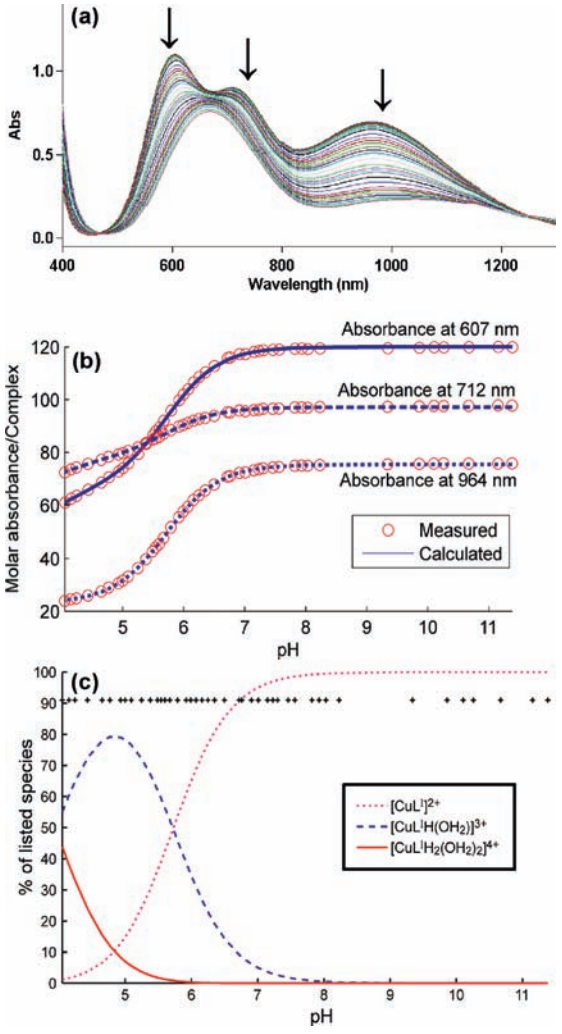

Figure 5. Changes in the UV−vis-NIR spectrum of complex **C1** as a function of pH, measured on a 9.28 mM aqueous solution of [**C1**]. (a) Series of UV−vis spectra; titration was commenced at pH 12, top spectrum, and finished at pH 4.0, bottom spectrum. (b) Evolution of molar absorbance at three wavelengths as a function of pH. Full lines show the absorbance calculated with the proposed speciation model (Scheme 2). (c) Species distribution diagram showing the variation in species present with pH for **C1**. Crosses at the top show the pH of measured solutions.

The species distribution profile calculated for the apparent stability constants indicates that for the Cu(II)−$\mathbf{L^1}$

Scheme 2. Plausible Model for Rationalizing the Changes in the Electronic Spectrum of **C1** with pH

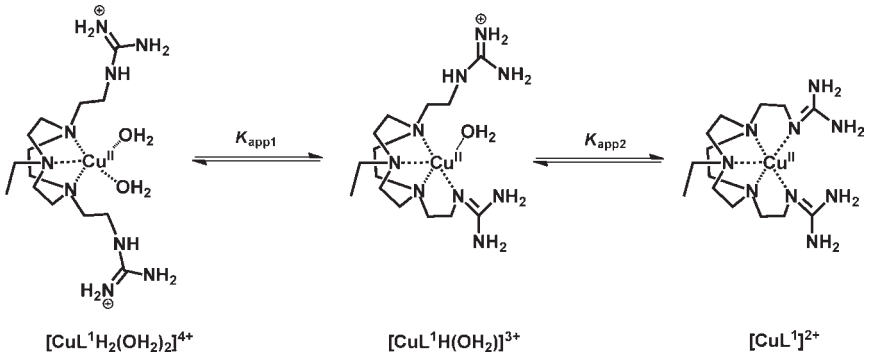

system, $[CuL^1]^{2+}$ is the only species present in significant concentration above pH 8 (Figure 5c). One explanation for the observed change in species distribution is that as the pH is decreased, detachment and protonation of one guanidine group occurs, possibly leading to a monoaqua complex, $[Cu(L^1H)(OH_2)]^{3+}$, with one protonated guanidine (dominant at ~pH 5), followed by formation of the complex with two protonated guanidines, $[Cu(L^1H_2)(OH_2)_2]^{4+}$, at the lower pH. We note, however, that the short Cu−N distance to the pendant guanidine nitrogens implies that these groups bind strongly to the copper(II) center.

The speciation for **C2** is more complex than for **C1**, as illustrated by Figure 6 and the principal component analysis (Figure S01, Supporting Information). In these plots, each factor corresponding to an actual absorbing species in solution causes a dramatic decrease in residuals, whereas additional factors only cause a small decrease.[63,78] In the case of the **C2** complex, the analysis of data sets obtained at constant ligand concentrations clearly shows the need for at least five factors to explain the series of spectra (Figure S01b, Supporting Information). The five species required to explain data set (b) may be related to the deprotonation of H_2O (three species) and NH_2 (two species) groups, as per Scheme 3. Note that this analysis cannot distinguish complexes of identical composition, e.g., $L^2Cu(NH_2)_2(OH)(OH_2)^{3+}$ from a complex in which pendant guanidinium groups hydrogen bond to the hydroxo group.

To test for the presence of polynuclear complexes, a second series of spectra were measured at a higher complex concentration (15 mM, see Figure 6a). The addition of a second data set at higher $[CuL^2]$ results in an increase in the number of factors from 5 to 6, suggesting the presence of polynuclear complexes (Figure S01c, Supporting Information). In contrast, additional factors were not required to describe the concentration dependence of **C1**, indicating the absence of polynuclear species. Analysis of the 5 mM data set using the five possible mononuclear species delivers an excellent fit (not shown). Different combinations of mono- and polynuclear species were

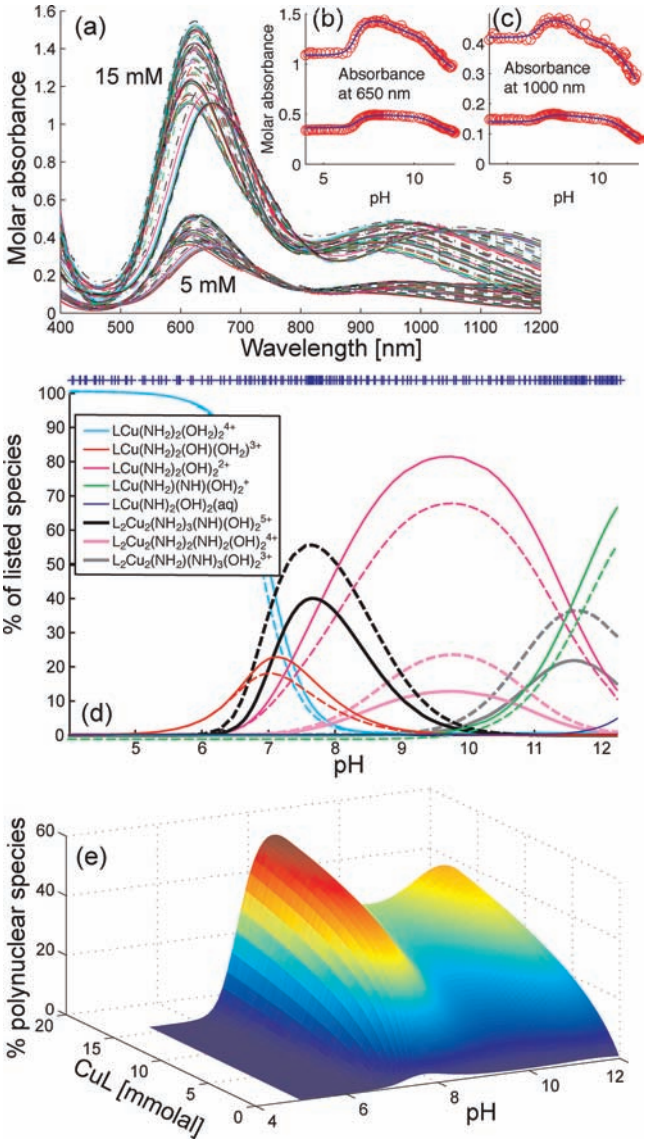

Figure 6. (a) Changes in the UV−vis-NIR spectrum of complex **C2** as a function of pH, measured on 5 and 15 mM aqueous solutions of **C2**. (b,c) Evolution of molar absorbance at two different wavelengths as a function of pH (the full lines show the absorbance calculated with the proposed speciation model, vide supra). (d) Speciation diagram showing the variation in species present with pH, crosses at the top show the pH of measured solutions, while the solid and dashed lines are for the 5 mM and 15 mM data sets. (e) Plot of the percent of polynuclear species as a function of pH and concentration of **C2**.

(76) Brudenell, S. J.; Spiccia, L.; Tieknik, E. D. T. *Inorg. Chem.* **1996**, *35*, 1974–1979.
(77) Belousoff, M. J.; Battle, A. R.; Graham, B.; Spiccia, L. *Polyhedron* **2007**, *26*, 344–355.
(78) Meloun, M.; Capek, J.; Miksik, P.; Brereton, R. G. *Anal. Chim. Acta* **2000**, *423*, 51–68.

Scheme 3. Plausible Model Rationalizing the Changes in the Electronic Spectrum of **C2** with pH and [**C2**]

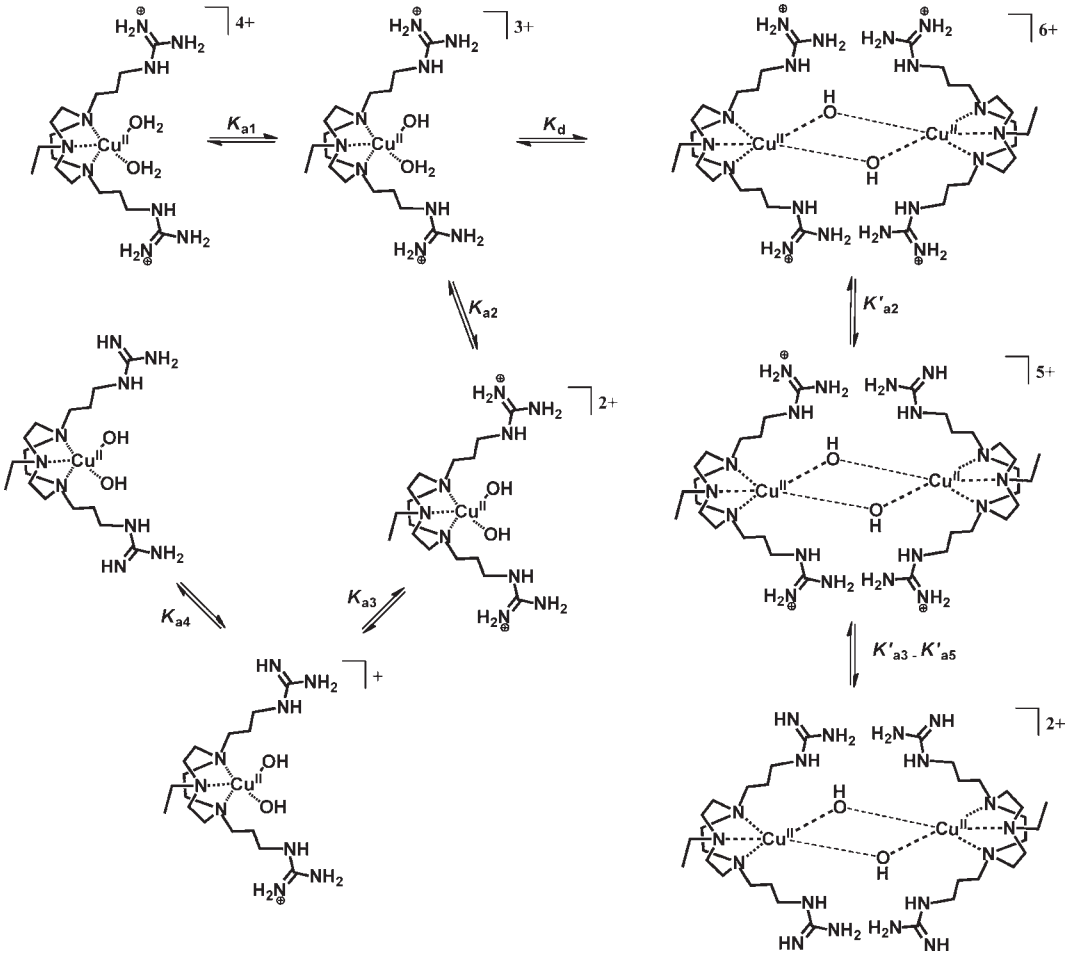

tested to explain the combined data set (5 and 15 mM), and the best results were obtained with a model including the five mononuclear species and three polynuclear species, $\mathbf{L^2}_2Cu_2(NH_2)_3(NH)(OH)_2^{5+}$, $\mathbf{L^2}_2Cu_2(NH_2)_2(NH)_2(OH)_2^{4+}$, and $\mathbf{L^2}_2Cu_2(NH_2)(NH)_3(OH)_2^{3+}$. The analysis provides the following constants:

$$\mathbf{L^2}Cu(NH_2)_2(OH_2)_2^{4+} = \mathbf{L^2}Cu(NH_2)_2(OH)(OH_2)^{3+} + H^+ \quad pK_{a1} = 7.00$$

$$\mathbf{L^2}Cu(NH_2)_2(OH)(OH_2)^{3+} = \mathbf{L^2}Cu(NH_2)_2(OH)_2^{2+} + H^+ \quad pK_{a2} = 7.68$$

$$\mathbf{L^2}Cu(NH_2)_2(OH)_2^{2+} = \mathbf{L^2}Cu(NH_2)(NH)(OH)_2^{+} + H^+ \quad pK_{a3} = 11.5$$

$$\mathbf{L^2}Cu(NH_2)(NH)(OH)_2^{+} = \mathbf{L^2}Cu(NH)_2(OH)_2(aq) + H^+ \quad pK_{a4} \sim 13.4$$

$$\mathbf{L^2}Cu(NH_2)_2(OH)_2^{2+} + \mathbf{L^2}Cu(NH_2)_2(OH)(OH_2)^{3+} = \mathbf{L^2}_2Cu_2(NH_2)_3(NH)(OH)_2^{5+} + 2H_2O \quad \log K_d = 2.97$$

$$2\mathbf{L^2}Cu(NH_2)_2(OH)_2^{2+} = \mathbf{L^2}_2Cu_2(NH_2)_2(NH)_2(OH)_2^{4+} + 2H_2O \quad \log K_d = 1.65$$

$$\mathbf{L^2}Cu(NH_2)_2(OH)_2^{2+} + \mathbf{L^2}Cu(NH_2)(NH)(OH)_2^{+} = \mathbf{L^2}_2Cu_2(NH_2)(NH)_3(OH)_2^{3+} + 2H_2O \quad \log K_d = 2.58$$

Note that this model includes eight species, while PCA shows that the data set can be explained using only six. This is only an apparent contradiction, since the distribution of the polynuclear species is highly correlated to that of the mononuclear species (Figure 6d). The fit quality is good, as shown in Figures 6b,c. On average, the difference between calculated and measured absorbances is 1%, and the highest discrepancies are 0.06 absorbance units. Careful observation of the data shows that these relatively high values are not related to the quality of the fit, but to higher experimental noise during **C2** titration (see, for example, Figure 6c).

The resulting distribution of species (Figure 6d) shows significant amounts of polynuclear complexes, with the highest proportion found at pH ~7.5, and increasing proportions also at high pH (> 11) (Figure 6e).

Binding of Model Phosphate Esters. To establish the effect of pH on the binding of model phosphate esters, the electronic spectrum of **C1** was recorded as a function of concentration of added *p*-nitrophenylphosphate (NPP) at

Table 4. First-Order Rate Constants for Hydrolysis of BNPP by Copper(II) Complexes of Tacn and Tacn Derivatives at pH 7.0 (Standard Error in Parentheses)[a]

compound	k_{obs} (s^{-1})	refs
control	3.00×10^{-10}	this work
Cu^{II}−tacn	$1.71(\pm0.01) \times 10^{-6}$	this work
C1[b]	$1.00(\pm0.03) \times 10^{-8}$	this work
C2	$7.24(\pm0.08) \times 10^{-5}$	this work
Cu^{II}−Me_2tacn[c]	1.24×10^{-5}	67
Cu^{II}−Me_3tacn[c]	3.7×10^{-5}	66
Cu^{II}−$^{i}Pr_3$tacn[c]	4.3×10^{-5}	66, 79
Cu^{II}−Et^{i}Prtacn[c]	1.43×10^{-5}	77
Cu^{II}−Bn^{i}Prtacn[c]	1.53×10^{-5}	77
Cu^{II}−BnMe$_2$tacn[c]	7.01×10^{-5}	67

[a] Abbreviations: Me_2tacn = 1,4-dimethyl-1,4,7-triazacyclononane, Me_3tacn = 1,4,7-trimethyl-1,4,7-triazacyclononane, $^{i}Pr_3$tacn = 1,4,7-triisopropyl-1,4,7-triazacyclononane, Et^{i}Prtacn = 1-ethyl-4-isopropyl-1,4,7-triazacyclononane, Bn^{i}Prtacn = 1-benzyl-4-isopropyl-1,4,7-triazacyclononane, Bn(Me_2)tacn = 1-benzyl-4,7-dimethyl-1,4,7-triazacyclononane. Conditions used: [complex] = 2 mM, [BNPP] = 0.1 mM, [HEPES] = 50 mM, I = 0.15 M, T = 50 °C). [b] Data were analyzed using the initial rate method, yielding k_{obs} indirectly, which was further converted to a first order rate constant. [c] Aqua complexes formed on dissolution in aqueous solution.

three pH values (6.0, 7.0 and 9.0). The spectrophotometric titrations for NPP are summarized in Supporting Information (Figure S02). At pH 9.0, no changes in the d−d electronic transitions of the complex were observed, even when a large excess of NPP was added. This indicates that NPP cannot displace the coordinated nitrogens from the copper(II) coordination sphere. At the lower pH values, a significant change in spectrum was observed, indicating that NPP is able to bind when aqua ligands occupy one or more metal coordination sites. From the variation in absorbance with [NPP] at the two wavelength maxima, 625 and 980 nm, the binding constants were calculated (see Experimental Section). At pH 6.0, the K_b value was found to be 34 (±1) M^{-1} while the corresponding K_b value at pH 7.0 was lower (14 (±2) M^{-1}) due to the lower concentration of the aqua complex available for complexation by NPP at this pH. In the case of **C2**, the change in spectrum on addition of NPP was small and did not allow the determination of K_b.

Hydrolysis of Model Phosphate Esters. Bis(*p*-nitrophenyl)phosphate (BNPP). To investigate the phosphate ester cleavage properties of **C1** and **C2**, their reactivity toward the widely employed activated phosphodiester, BNPP, was explored by monitoring the release of the highly colored *p*-nitrophenoxide anion, (λ_{max} = 400 nm). The rates of BNPP cleavage by 2 mM solutions of **C1**, **C2**, and, for comparison, $[Cu(tacn)(OH_2)_2]^{2+}$, measured at pH 7.0 and T = 50 °C, are summarized in Table 4. Interestingly, **C1** was found to be significantly less effective in cleaving BNPP than the parent complex, $[Cu(tacn)(OH_2)_2]^{2+}$, under the conditions of our study. At lower and higher pH values, no release of NP could be detected by spectrophotometry even after seven days, which meant that the reaction was too slow for rate constants to be determined. This was anticipated from the speciation profile, which showed that the coordination sphere of the dominant complex is occupied by strong donor atoms. In contrast, the rate of BNPP cleavage by **C2** is 300-times faster than for **C1** and 30-times faster than for $[Cu(tacn)(OH_2)_2]^{2+}$. Consequently, investigation of **C1** was less

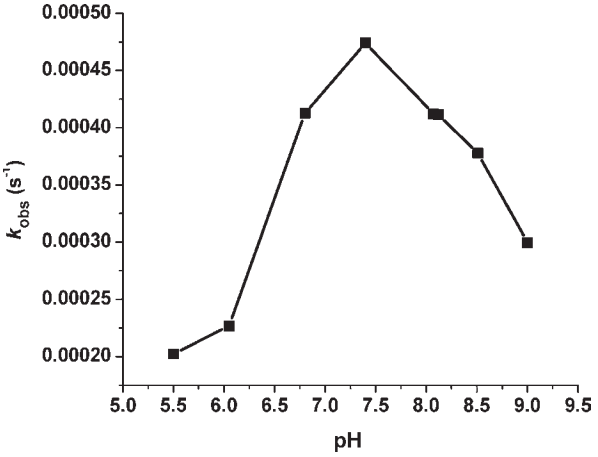

Figure 7. pH dependence of the rate of hydrolysis of BNPP by **C2** at 50 °C ([**C2**] = 4 mM, [BNPP] = 0.1 mM).

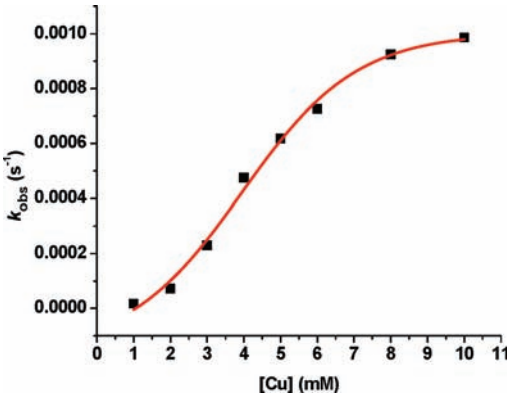

Figure 8. Complex concentration dependence profile for the hydrolysis of BNPP by **C2** at pH 7.0 and T = 50 °C ([**C2**] = 1−10 mM, [BNPP] = 0.1 mM).

detailed than for **C2**. The greater activity of **C2** could be the result of activation of the phosphate ester or stabilization of transition states through electrostatic/hydrogen-bonding interactions with the guanidine pendants, or a restriction in the formation of inactive dihydroxo-bridged copper(II) dimers by *N*-functionalization of the tacn macrocycle.[66,67,77,79] In comparison with *N*-alkylation of the tacn macrocycle, the introduction of positively charged guanidinium pendants (**C2**) does not further enhance the rate of BNPP hydrolysis, suggesting that the pendant guanidinium groups have only marginal influence (Table 4).

Further investigation of the kinetics of BNPP hydrolysis by **C2** was undertaken to examine the effect of complex concentration and pH on the rate of hydrolysis. The pH dependence of the rate of BNPP hydrolysis follows a bell-shaped profile (Figure 7), similar to the profiles reported by other groups.[80−82] As in previous studies, this pH dependence can be proposed to arise from the relative activity of the species formed on successive

(79) Deck, K. M.; Tseng, T. A.; Burstyn, J. N. *Inorg. Chem.* **2002**, *41*, 669–677.
(80) Chapman, J., W. H.; Breslow, R. *J. Am. Chem. Soc.* **1995**, *117*, 5462–5469.
(81) Young, M. J.; Chin, J. *J. Am. Chem. Soc.* **1995**, *117*, 10577–10578.
(82) Mancin, F.; Rampazzo, E.; Tecilla, P.; Tonellato, U. *Eur. J. Org. Chem.* **2004**, *2004*, 281–288.

Table 5. First-Order Rate Constants for Hydrolysis of HPNPP by Copper(II) Complexes at pH 7.0 (Standard Error in Parentheses)[a]

compound	k_{obs} (s^{-1})	refs
control	$1.2\,(\pm0.7) \times 10^{-8}$	this work
Cu^{II}–tacn	$3.58\,(\pm0.2) \times 10^{-6}$	this work
C1	$1.3\,(\pm0.6) \times 10^{-7}$	this work
C2	$3.2\,(\pm0.3) \times 10^{-5}$	this work
Cu^{II}–**D**[b]	1.53×10^{-5}	84
Cu^{II}–**E**[b]	3.89×10^{-5}	84
Zn^{II}–**F**[c]	4.6×10^{-5}	54

[a] Conditions used: [complex] = 2 mM, [HPNPP] = 0.1 mM, [HEPES] = 50 mM, I = 0.15 M, T = 25 °C. Data were analyzed using first-order analysis, yielding k_{obs} directly. [b] [complex] = 2 mM, [HPNPP] = 0.2 mM at 25 °C, pH 7.0. [c] [complex] = 1 mM.

deprotonations of the two coordinated aqua ligands. The first deprotonation (K_{a1}) forms a monohydroxo monoaqua complex, which is proposed to be active and responsible for the increase in reaction rate to a maximum at pH 7.4, but exists in equilibrium with an inactive dihydroxo-bridged dimer, whose concentration depends on the magnitude of the dimerization constant, K_{DIM}. The second deprotonation (K_{a2}) generates a mononuclear dihydroxo complex which is poorly active as coordination and activation of the phosphate ester involves displacement of a hydroxo ligand. Consequently, a significant decrease in rate is observed above pH 7.4.

The rate of BNPP hydrolysis increases with **C2** concentration (Figure 8), reaching saturation at the higher concentrations (10 mM). This behavior is similar to that exhibited by a variety of other *cis*-diaqua copper(II) complexes,[46,83] where the reactivity of phosphate ester hydrolysis levels off with increasing concentrations of complex, due to the dimerization of metal complexes. Spectrophotometric pH titration of **C2** indicates the presence of the dihydroxo-bridged dimer, $[\mathbf{L^2}Cu_2(NH_2)_3(NH)(OH)_2]^{5+}$ at pH 7.0, which was found to increase with increasing complex concentration (see Figure 6d,c). The speciation data for **C2** was used to estimate the concentration of the monohydroxo complex, $[\mathbf{L^2}Cu(NH_2)_2(OH)(OH_2)]^{3+}$, as a function of [**C2**]. The linear dependence of k_{obs} on the concentration of this species supports the view that this is the active species in BNPP hydrolysis (see Figure S03 and Table S02, Supporting Information), from which the second order rate constant for cleavage of BNPP by $[\mathbf{L^2}Cu(NH_2)_2(OH)(OH_2)]^{3+}$ was estimated. The value of 1.5 $M^{-1}\,s^{-1}$ is higher than the values of 0.135, 0.060, and 0.0002 $M^{-1}\,s^{-1}$ determined at 50 °C for $[(Me_3tacn)Cu(OH)(OH_2)]^+$, $[(^iPr_3tacn)Cu(OH)(OH_2)]^+$ and $[(tacn)Cu(OH)(OH_2)]^+$, respectively.[66]

2-Hydroxypropyl-*p*-nitrophenylphosphate (HPNPP). The rate of cleavage of an RNA model, HPNPP, by **C1** and **C2** was measured at pH 7.0 at 25 °C (Table 5). As for RNA, this compound undergoes hydrolysis via an intramolecular transesterification reaction, involving nucleophilic attack of the 2′–OH, to form a cyclic diester and the highly colored *p*-nitrophenolate chromophore, which can be monitored by spectrophotometry (see Experimental Section). The nonfunctionalized parent complex, $[Cu(tacn)(OH_2)_2]^{2+}$ was itself found to cleave HPNPP 300 times faster than the control. By comparison, **C2** accelerates the rate of cleavage of HPNPP 10-fold when compared to $[Cu(tacn)(OH_2)_2]^{2+}$ and 3000 times relative to the control at the same pH. As for the hydrolysis of BNPP, **C1** was found to be significantly less effective in cleaving HPNPP than $[Cu(tacn)(OH_2)_2]^{2+}$ because of its inability to coordinate the substrate, a critical first step in the activation of the phosphate diester toward hydrolysis. The increased rate of cleavage of HPNPP by **C2** compared to $[Cu(tacn)(OH_2)_2]^{2+}$ reflects similar findings reported in the literature. For instance, Hamilton and co-workers[84] found that introduction of peripheral tertiary amino groups into a Cu(II)–terpy complex (Figure 9, complexes **D** and **E**) increased HPNPP cleavage activity by 3–7-fold. More impressively, Williams et al.[54] have reported a zinc(II) complex with appended amino groups (Figure 9, complex **F**) that cleaves HPNPP 1.5×10^3-times faster than the parent complex lacking any amino groups. These findings clearly indicate that cooperativity between metal ions and proximal functional groups can effectively enhance the rate of phosphodiester hydrolysis.

In our case, the speciation data for **C2** allows the estimation of a second-order rate constant of 0.9 ± 0.1 $M^{-1}\,s^{-1}$ for the cleavage of HPNPP by $[\mathbf{L^2}Cu(NH_2)_2(OH)(OH_2)]^{3+}$.

Cleavage of Plasmid DNA. The ability of the copper(II) complexes of $\mathbf{L^1}$ and $\mathbf{L^2}$ to cleave nucleic acids was probed using plasmid pBR 322 DNA as a model system. DNA cleavage was measured by the conversion of the supercoiled form of the plasmid DNA (Form I) to the nicked circular form (Form II). The doubly nicked linear form (Form III) was not observed in this study. Experiments were conducted in which pBR 322 plasmid DNA (38 μM base pair concentration) was incubated with an excess of **C1** and **C2** (75–600 μM) (pseudo-first-order conditions) for varying time intervals, under near physiological conditions (pH 7.0 and T = 37 °C) and at variable pH (see Figure 10A and Supporting Information Figures S04–S08). Cleavage experiments were also performed with $[Cu(tacn)(OH_2)_2]^{2+}$, to assess whether the guanidinium groups in **C1** and **C2** lead to enhanced DNA cleavage activity (see Figure 10A and Supporting Information Figure S08).

Typical images of the electrophoresis gels obtained from the incubated reaction mixtures are shown in Figure 10A. For all complexes, a decrease in the intensity of the band due to Form I with incubation time was accompanied by the appearance and intensification of a band corresponding to Form II of the plasmid DNA. This demonstrates the ability of the complexes to create single nicks in plasmid pBR 322 DNA. The extent of cleavage was found to be somewhat greater for the complexes bearing guanidinium pendant groups. After 24 h incubation at pH 7.0, 60–75% of the initial pBR 322 plasmid DNA added to solutions containing 150 μM of **C1** and **C2** was converted to Form II, *cf.*, 40% for the non-functionalized $[Cu(tacn)(OH_2)_2]^{2+}$ complex. This enhanced DNA cleavage activity is reflected in the higher observed first-order rate constants, k_{obs}, for **C1** and **C2** {for typical examples of the data and kinetic profiles see in Supporting Information Figures S09–S11 and Tables S03–S05,

(83) Sissi, C.; Mancin, F.; Gatos, M.; Palumbo, M.; Tecilla, P.; Tonellato, U. *Inorg. Chem.* **2005**, *44*, 2310–2317.

(84) Liu, S.; Hamilton, A. D. *Tetrahedron Lett.* **1997**, *38*, 1107–1110.

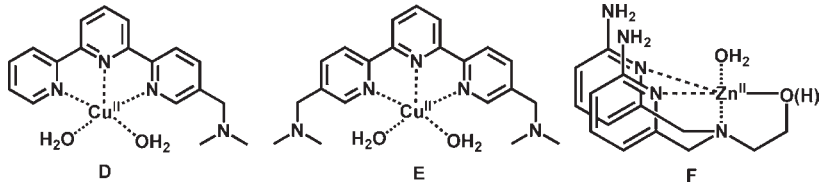

Figure 9. Examples of complexes with amino group pendants that accelerate HPNPP cleavage.

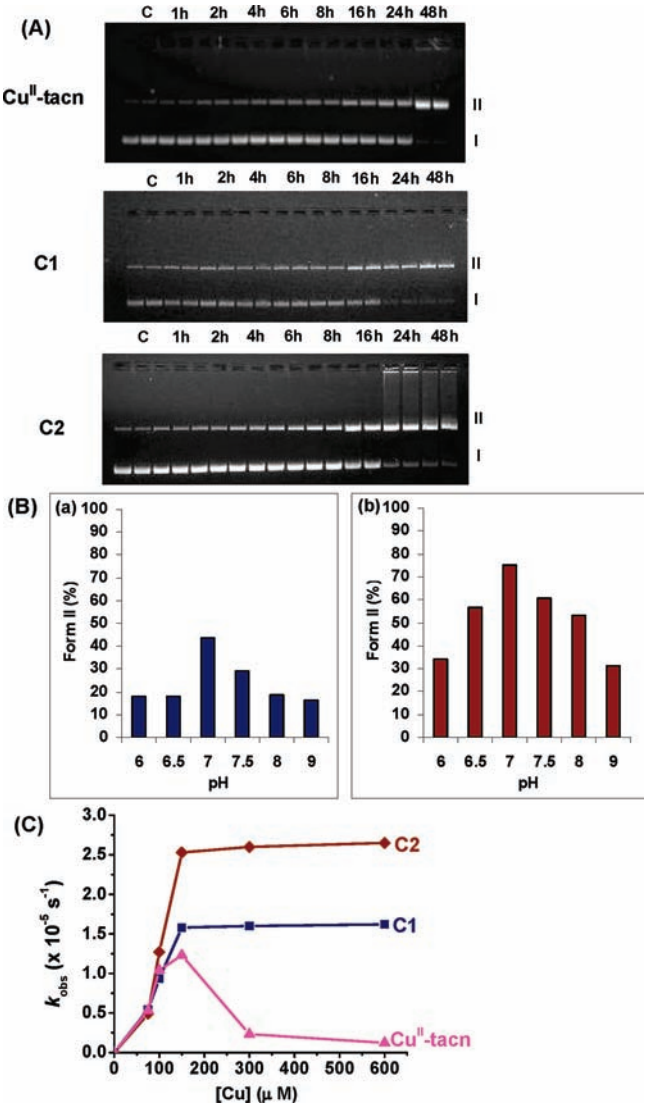

Figure 10. (A) Agarose gels showing cleavage of pBR 322 plasmid DNA (38 μM bp) by Cu^{II}−tacn, **C1**, and **C2** (150 μM) in HEPES buffer (40 mM, pH 7.0) at 37 °C for various time intervals. Lane 1 and 2: DNA control, lane 3 and 4: 1 h, lane 5 and 6: 2 h, lane 7 and 8: 4 h, lane 9 and 10: 6 h, lane 11 and 12: 8 h, lane 13 and 14: 16 h, lane 15 and 16: 24 h, lane 17 and 18: 48 h. (B) The pH dependence of the cleavage of pBR 322 DNA by **C1** (a) and **C2** (b) after 4 h of incubation ([DNA] = 38 μM bp, [complex] = 150 μM, I = 0.15 M and T = 37 °C). (C) Concentration dependence of cleavage of pBR 322 DNA promoted by Cu^{II}−tacn, **C1** and **C2** in 40 mM HEPES (pH 7.0) at 37 °C over a defined time intervals.

and see Table 6 and Supporting Information Tables S06−S07 for summaries of k_{obs} values}. Control experiments confirmed that no measurable DNA cleavage occurs when pBR 322 plasmid DNA is incubated with either 150 μM of the non-metalated ligands or and 150 μM $CuCl_2$ (see Supporting Information Figure S12). This indicates

Table 6. Observed Rate Constant, k_{obs}, for Single-Strand Cleavage of pBR 322 Plasmid DNA by Copper(II) Complexes at pH 7.0 (Standard Error in Parentheses)[a]

Compound	k_{obs} (s^{-1})	refs
Cu^{II}−tacn	$1.23\ (\pm 0.37) \times 10^{-5}$	this work
Cu^{II}−tacn[b]	1.5×10^{-5}	14
C1	$1.54\ (\pm 0.32) \times 10^{-5}$	this work
C2	$2.60\ (\pm 0.71) \times 10^{-5}$	this work
Cu^{II}−**G**[c]	3.61×10^{-6}	59
Zn^{II}−**H**[d]	1.13×10^{-5}	85
Cu^{II}−**I**	8.50×10^{-4}	57
Cu^{II}−**J**	2.39×10^{-4}	58

[a] Conditions used: [complex] = 150 μM, [pBR 322 plasmid] = 38 μM (per bp), [HEPES] = 40 mM (pH 7.0 at 37 °C. Data were analyzed using first-order analysis, yielding k_{obs} directly. [b] [complex] = 25 μM at 50 °C, pH 7.8. [c] [complex] = 100 μM. [d] [complex] = 144 μM.

that the species active in DNA cleavage are (or are derived) from the metal complexes, **C1** and **C2**.

In contrast to the BNPP and HPNPP cleavage results, complex **C1** was found to cleave DNA at a similar rate to $[Cu(tacn)(OH_2)_2]^{2+}$. Synthetic metallonucleases are suggested to promote phosphate ester hydrolysis via intramolecular attack on the substrate by a metal-coordinated hydroxide. Therefore, to be an effective nuclease, the metal complex should have sites available for substrate binding as well as for binding water or hydroxide.[6] The speciation distribution curve (Figure 5c) shows that at pH 7.0, **C1** (or $[Cu\mathbf{L^1}]^{2+}$) constitutes 95% of the total complex concentration at pH 7, indicating that only 5% of the monoaqua complex, $[Cu(\mathbf{L^1}H)(OH_2)]^{3+}$, is present. Assuming that **C1** itself is inactive, and given that there is a large excess of complex present relative to the DNA concentration, it can then be postulated that $[Cu(\mathbf{L^1}H)(OH_2)]^{3+}$ is the active DNA cleavage agent. The involvement of $[Cu(\mathbf{L^1}H_2)(OH_2)_2]^{4+}$ is unlikely due to the very low concentration of this species expected at pH 7. On introduction of the DNA, the negatively charged phosphate groups on the DNA backbone will interact with the pendant guanidinium groups and a series of complex equilibria will be established in solution. Depending on the strength of the DNA phosphate-guanidinium interactions and the DNA phosphate-Cu(II) coordinative interaction, detachment and protonation of the coordinated guanidine could occur, which would have the consequence of "activating" the cleavage process. We note that the initial DNA cleavage process involves a single nick that converts the supercoiled DNA into the relaxed circular form (Form II), which could potentially be achieved by the action of a single metal center.

The rate of DNA cleavage by **C2** was faster than that for both **C1** and $[Cu(tacn)(OH_2)_2]^{2+}$. As indicated above, the solution speciation of **C2** is much more complex, with mononuclear and binuclear complexes coexisting in the same pH range, as has been established previously for

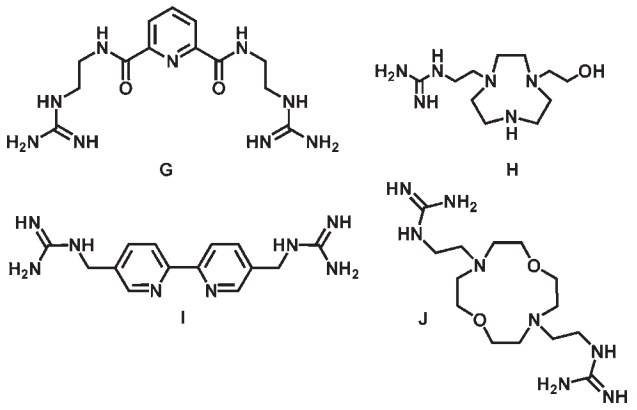

Figure 11. Selected ligands with guanidine pendants whose complexes accelerate DNA cleavage.

these types of Cu(II)-tacn complexes.[66,67,77,79] The higher rates of cleavage of the model phosphate esters and DNA by this complex, therefore, suggests that either more active monomeric species are present in solution or that the cleavage reactions are promoted by cooperative interactions with the charged guanidinium groups.

A modest DNA cleavage activity was achieved by complexes **C1** and **C2** compared to cleavage agents reported by other groups (Table 6 and Figure 11).[57−59,81] Both cleave DNA an order of magnitude faster than the Cu(II) complex of ligand **G**, which bears pairs of guanidinoethyl pendants on an acyclic backbone.[59] A tacn macrocycle with guanidinoethyl and alcohol pendants (**H**)[85] exhibited slightly higher cleavage rate (3.64×10^{-5} s^{-1}), in the absence of any metal, compared to both **C1** and **C2**. However, the cleavage activity was lower for the corresponding Zn(II)−**H** complex.[85] This highlights the uncertainty that exists about the factors responsible for promoting metal-guanidine assisted DNA cleavage. Further, incorporation of the guanidine pendant into a rigid aromatic scaffold (Cu^{II}-**I** complex)[57] rather than linking them by a flexible alkyl chain, as in **C1** and **C2** or on a larger macrocycle (Cu^{II}−**J**)[58] results in faster DNA cleavage. This suggests that both the rigidity of the guanidine pendant arm and the stability of the Cu(II)−guanidine complex are crucial factors in determining the cleavage activity.

pH-Dependence of DNA cleavage. To investigate the effect of solution pH on the rate of DNA cleavage, cleavage experiments were performed in various buffer solutions (40 mM) over the pH range of 6.0−9.0. Typical DNA electrophoresis gels are shown in Figures S04 and S05 in the Supporting Information. For both **C1** and **C2**, the variation in cleavage with pH was measured at a complex concentration of 150 μM and after a reaction time of 4 h. The plot of percentage cleavage versus pH displays a bell-like profile (Figure 10b), with an optimal pH for DNA cleavage of 7.0 for both **C1** and **C2**. This pH-dependent cleavage behavior is very similar to that reported in the literature for related complexes.[37,58] In the case of **C1**, the decrease in the cleavage activity at high pH can be attributed to conversion of the complex to the inactive $[CuL^1]^{2+}$ species (see speciation profile in Figure 5 and Scheme 2), which has a fully saturated coordination sphere and is therefore incapable of coordinating the phosphate groups on DNA. For **C2**, mononuclear complexes will be converted into the corresponding dihydroxo complexes as the pH increases (see Scheme 3), which for similar reasons as for **C1** are expected to be inactive.

Effect of Complex Concentration on DNA Cleavage. The concentration dependence of DNA cleavage by **C1**, **C2** and $[Cu(tacn)(OH_2)_2]^{2+}$ at the pH of optimum activity is shown in Figure 10c (for typical DNA electrophoresis gels, see Figures S06−S08 in Supporting Information). At lower concentrations (< 100 μM), all three complexes showed similar cleavage rates, indicating minimal effect from the guanidine pendants. At 150 μM, however, **C2** showed significantly greater cleavage activity ($k_{obs} = 2.60 \times 10^{-5}$ s^{-1}) than both **C1** (1.54×10^{-5} s^{-1}) and $[Cu(tacn)(OH_2)_2]^{2+}$ (1.23×10^{-5} s^{-1}). Increasing the concentration beyond 150 μM produced little change in the activity of **C1** or **C2**, while a significant decrease in rate was observed for $[Cu(tacn)(OH_2)_2]^{2+}$. The saturation profile seen for **C1** and **C2** is observed quite often for biomolecular reactions, and has been previously reported for the cleavage of DNA by copper(II) complexes.[86−88] On the other hand, the profile measured for $[Cu(tacn)(OH_2)_2]^{2+}$ has previously been tentatively attributed to increased formation of dihydroxo-bridged dimers at higher concentration, which bind to the DNA and block access of the cleavage-active monomeric species.[66,67,77,79]

Effect of Reactive Oxygen Species on DNA Cleavage. DNA cleavage by copper(II) complexes can be achieved through hydrolytic[83,89−91] as well as oxidative[92−94] pathways. Reactive oxygen species (ROS) generated from the interaction of the copper(II) complexes with dioxygen are believed to be a key factor in DNA cleavage.[21,95,96] To investigate whether ROS, such as singlet oxygen and hydroxyl radicals, were involved in DNA cleavage by **C1** and **C2**, reactions were carried out in the presence of scavengers for hydroxyl radical (10 mM KI, DMSO or ^{t}BuOH) or singlet oxygen (10 mM NaN_3), as has been reported previously in the literature.[42,58,59] As shown in Supporting Information Figures S13−S15 and Tables S08−S09, no obvious inhibition of cleavage activity was observed in the presence of the singlet oxygen scavenger, sodium azide, or the hydroxyl radical scavengers, DMSO and ^{t}BuOH, which indicates that these species are not likely to be involved in DNA cleavage. However, the

(85) Sheng, X.; Lu, X. M.; Zhang, J. J.; Chen, Y. T.; Lu, G., -Y.; Shao, Y.; Liu, F.; Xu, Q. *J. Org. Chem.* **2007**, *72*, 1799–1802.

(86) Schwarzenbach, G.; Boesch, J.; Egli, H. *J. Inorg. Nucl. Chem.* **1971**, *33*, 2141–2156.

(87) Burstyn, J. N.; Deal, K. A. *Inorg. Chem.* **1993**, *32*, 3585–3586.

(88) Basile, L. A.; Raphael, A. L.; Barton, J. K. *J. Am. Chem. Soc.* **1987**, *109*, 7550–7551.

(89) Gupta, T.; Dhar, S.; Nethaji, M.; Chakravarty, A. R. *Dalton Trans.* **2004**, 1896–1900.

(90) Kirin, S. I.; Happel, C. M.; Hrubanova, S.; Weyhermuller, T.; Klein, C.; Metzler-Nolte, N. *Dalton Trans.* **2004**, 1201–1207.

(91) Zhu, L.; dos Santos, O.; Koo, C. W.; Rybstein, M.; Pape, L.; Canary, J. W. *Inorg. Chem.* **2003**, *42*, 7912–7920.

(92) Singh, U. S.; Scannell, R. T.; An, H.; Carter, B. J.; Hecht, S. M. *J. Am. Chem. Soc.* **1995**, *117*, 12691–12699.

(93) Abraham, A. T.; Zhou, X.; Hecht, S. M. *J. Am. Chem. Soc.* **2001**, *123*, 5167–5175.

(94) Wagner, C.; Wagenknecht, H., -A. *Chem.—Eur. J.* **2005**, *11*, 1871–1876.

(95) Thyagarajan, S.; Murthy, N. N.; Narducci, S., A. A.; Karlin, K. D.; Rokita, S. E. *J. Am. Chem. Soc.* **2006**, *128*, 7003–7008.

(96) Pyle, A. M.; Barton, J. K. *Prog. Inorg. Chem.* **1990**, *38*, 413.

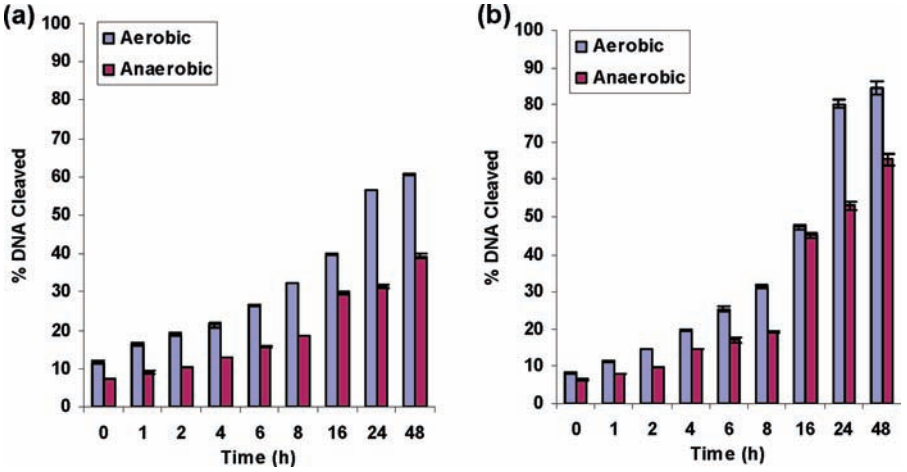

Figure 12. Extent of aerobic and anaerobic cleavage of pBR 322 plasmid DNA by **C1** (a) and **C2** (b) [**C1**] and [**C2**] = 150 μM in 40 mM HEPES (pH 7.0) at 37 °C over defined time intervals.

addition of the hydroxyl radical scavenger, KI, resulted in substantial inhibition of DNA cleavage. On the basis of this observation, the mechanism of DNA cleavage mediated by **C1** and **C2** may be similar to that proposed for other multinuclear copper complexes,[97−100] whereby DNA cleavage is redox-mediated − Cu(II) centers are initially reduced to Cu(I) species and, subsequently, react with dioxygen to form peroxo-dicopper(II) derivatives, which in turn generate active oxygen species necessary for cleavage. However, although widely used it should be noted that an excess of iodide is capable of reducing the copper(II) complexes to the corresponding copper(I) complexes, and then displacing the ligands from the complex, leading to the precipitation of CuI.[101]

Anaerobic Cleavage of DNA. To further probe the effects of molecular oxygen on the degradation of DNA by the copper(II) complexes of $\mathbf{L^1}$ and $\mathbf{L^2}$, reactions were also performed under rigorously anaerobic condition. Both **C1** and **C2** were found to still effectively cleave supercoiled plasmid pBR 322 plasmid DNA, although the rate of the hydrolysis was significantly reduced (~30%) when compared to that observed under aerobic condition (Figures 12 and Supporting Information Figures S16−S17 and Tables S10−S11). These results are similar to those obtained for $[Cu(tacn)(OH_2)_2]^{2+}$ by Burstyn and co-workers,[14] indicating the simultaneous occurrence of a prevailing hydrolytic cleavage pathway and an oxidative cleavage pathway.

Conclusion

Two new derivatives of 1,4,7-triazacyclononane featuring pairs of ethylguanidine ($\mathbf{L^1}$) and propylguanidine ($\mathbf{L^2}$) pendant arms are reported. An X-ray structure determination of $[Cu\mathbf{L^1}](ClO_4)_2$, revealed the unexpected coordination of the pendant guanidine groups. The quite short Cu−N distances of 2.0 Å, compare and estimated binding constants of $>10^6$ for each guanidine indicate remarkably stable Cu−N(guanidine) bonds. Of the two complexes, **C2** was a more effective cleavage agent for the model phosphate esters, BNPP and HPNPP, than the non-functionalized parent complex, $[Cu(tacn)(OH_2)_2]^{2+}$, while **C1** was essentially inactive. In contrast, DNA cleavage experiments indicated that both complexes enhance the cleavage of DNA relative to $[Cu(tacn)(OH_2)_2]^{2+}$, but it is unclear whether this is a direct result of the introduction of the positively charged guanidinium groups. The complexes showed cleavage activity toward plasmid DNA under both aerobic and anaerobic conditions, with a ~30% decrease in reactivity observed under anaerobic condition, indicating that cleavage occurs through both hydrolytic and redox pathways.

Acknowledgment. This work was supported by the Australian Research Council through the Discovery Program. L.T. is the recipient of a Monash Graduate Scholarship.

Supporting Information Available: Crystallographic file in CIF format, table of crystallographic data (Table S01), principal component analysis (PCA) (Figure S01), UV−vis-NIR spectra of complex **C1** titrated against NPP (Figure S02), analysis of kinetics of BNPP cleavage (Figure S03 and Table S02), and agarose gel images of DNA cleavage and kinetic profiles (Figures S04−S17 and Tables S03−S11). This material is available free of charge via the Internet at http://pubs.acs.org.

(97) Humphreys, K. J.; Karlin, K. D.; Rokita, S. E. *J. Am. Chem. Soc.* **2002**, *124*, 6009–6019.
(98) Humphreys, K. J.; Karlin, K. D.; Rokita, S. E. *J. Am. Chem. Soc.* **2001**, *123*, 5588–5589.
(99) Humphreys, K. J.; Karlin, K. D.; Rokita, S. E. *J. Am. Chem. Soc.* **2002**, *124*, 8055–8066.
(100) Humphreys, K. J.; Johnson, A. E.; Karlin, K. D.; Rokita, S. E. *J. Biol. Inorg. Chem.* **2002**, *7*, 835–842.
(101) Cotton, F. A.; Wilkinson, G. *Advanced Inorganic Chemistry*; 6th ed.; John Wiley & Sons: New York, 1999.